NUMERICAL STUDY OF TAYLOR BUBBLE BREAKUP BY PLACING OBSTACLE AT T-JUNCTION BIFURCATION

A THESIS SUBMITTED IN PARTIAL FULLFILLMENT OF THE REQUIREMENTS

FOR THE DEGREE OF

Master of Technology

in

Mechanical Engineering

By

SANGRAM KUMAR SAMAL

Roll No: 213ME3438

DEPARTMENT OF MECHANICAL ENGINEERING
NATIONAL INSTITUTE OF TECHNOLOGY ROURKELA
ROURKELA-769008
JUNE-2015

NUMERICAL STUDY OF TAYLOR BUBBLE BREAKUP BY PLACING OBSTACLE AT T-JUNCTION BIFURCATION

A THESIS SUBMITTED IN PARTIAL FULLFILLMENT OF THE REQUIREMENTS

FOR THE DEGREE OF

Master of Technology

in

Mechanical Engineering

By

SANGRAM KUMAR SAMAL

Roll No: 213ME3438

Under the guidance of

Dr. MANOJ KUMAR MOHARANA

DEPARTMENT OF MECHANICAL ENGINEERING
NATIONAL INSTITUTE OF TECHNOLOGY ROURKELA
ROURKELA-769008
JUNE-2015

NATIONAL INSTITUTE OF TECHNOLOGY ROURKELA

CERTIFICATE

This is to certify that the thesis entitled, "**NUMERICAL STUDY OF TAYLOR BUBBLE BREAKUP BY PLACING OBSTACLE AT T-JUNCTION BIFURCATION**" submitted by **Mr. Sangram Kumar Samal** in partial fulfillment of the requirements for the award of **Master of Technology** Degree in **Mechanical Engineering** with specialization in **Thermal Engineering** at the National Institute of Technology Rourkela is an authentic work carried out by him under my supervision and guidance.

To the best of my knowledge, the matter embodied in the thesis has not been submitted to any other University/Institute for the award of any degree or diploma.

28/05/2015

Dr. Manoj Kumar Moharana
Assistant Professor
Department of Mechanical Engineering
National Institute of Technology Rourkela
Rourkela - 769008

Date: 28 May 2015

SELF DECLARATION

I, Mr Sangram Kumar Samal, Roll No. 213ME3438, student of M.Tech (2013-2015), Thermal Engineering at Department of Mechanical Engineering, National Institute of Technology Rourkela do hereby declare that I have not adopted any kind of unfair means and carried out the research work reported in this thesis work ethically to the best of my knowledge. If adoption of any unfair means is found in this thesis work at a later stage, then appropriate action can be taken against me including withdrawal of this thesis work.

NIT Rourkela
Date: 28/5/2015

Sangram Kumar Samal

Sangram Kumar Samal

ACKNOWLEDGEMENT

I would like to express my sincere gratitude and thanks to my project guide Dr. Manoj Kumar Moharana (Assistant Professor, Department of Mechanical Engineering) for his extensive support and inspiring guidance towards the progress of my project topic "Numerical study of Taylor bubble breakup by placing obstacle at T-junction bifurcation". His valuable suggestions and constant encouragement helped me to complete the project work successfully. Working under him has indeed been a great experience and inspiration for me.

I would like to thank Mechanical Engineering Department for providing the CFD lab, where I completed the maximum part of my project work. I am also very much thankful to National Institute of Technology for giving High Performance Computing (HPC) facility, through which I complete all my simulations.

I finally expressed my sincere gratitude to all those who have directly or indirectly helped me in completing this project work.

Place: NIT Rourkela
Date: 28/5/2015

Sangram Kumar Samal

Sangram Kumar Samal

ABSTRACT

A two-dimensional numerical study of Taylor bubble breakup is carried out, where Taylor bubble flows in a horizontal T- section microchannel with T-junction bifurcation. The numerical simulation is carried out by using the Volume-of-Fluid (VOF) multiphase model in ANSYS Fluent®. The Taylor bubble is formed at the upstream T-junction where air and water enter through two inlets perpendicular to each other. At the end of the channel, the Taylor bubble breaks up into two equal sizes at the bifurcated T junction. For controlled breakup of the Taylor bubble into two unequal lengths, an obstacle is positioned at the T-junction bifurcation to which the Taylor bubble strikes. The bubble breakup will be symmetrical, asymmetrical or no breakup depending on the position and height of the obstacle. In this work the obstacle position varied from X = 0 to 0.1 mm, where X is the distance from the center of T-junction bifurcation to the obstacle and height, is varied from Y = 0.05 to 0.2 mm. When X = 0 (i.e. the obstacle is positioned at the center), the symmetrical bubble breakup occurs and when X > 0 asymmetrical bubble breakup occurs. When the bubble breaks into unequal lengths, the length of the bifurcated bubble is higher along the outlet path opposite to that of the obstacle positioned. In this work, some parameters are calculated such as bubble length ratio, breakup length, breakup time and pressure drop. The result reveals that the bubble length ratio decreases as the obstacle height increases for a particular position of the obstacle. Similarly the breakup length and the breakup time decreases as the obstacle height increases for a particular obstacle position. From the results, it also observed that the pressure drop increases as the obstacle height increases for a particular position of the obstacle.

Keywords: Taylor bubble, microchannel, T-junction bifurcation, bubble breakup, two phase.

Contents

List of Figures

Nomenclature

C	Courant number
Ca	Capillary number
Re	Reynolds number
$\vec{F}$	Surface tension force of the liquid, N/m^2
$\vec{v}$	Velocity vector, m/s
u	Magnitude of velocity, m/s
P	Pressure force, N/m^2
D_h	Hydraulic diameter of the channel, mm
R	Channel radius, mm
X	Position of obstacle, mm
Y	Height of obstacle, mm
t	Time, s
C_p	Specific heat at constant pressure, J/kg-K
k_f	Thermal conductivity, W/m-K
p*	Dimensionless pressure drop
p_i	Pressure at the inlet to the T-junction bifurcation, pas
p_l	Pressure at the left side branch of the T-junction bifurcation, pas
p_r	Pressure at the right side branch of the T-junction bifurcation, pas

Greek symbol

ρ	Density, kg/m^3
μ	Dynamic viscosity, $N–s/m^2$
σ	Coefficient of surface tension, N/m

δ	Liquid film thickness between wall and bubble, mm
α	Volume fraction
∇	Differential operator
Δt	Time step size, s
Δx	Length interval, mm

Subscript

L	Liquid
G	Gas

Superscript

T	Transpose

Chapter-1

Introduction

Microfluidics is defined as the science and technology of the systems which operates small volumes of fluids in channels having dimensions in between 0.001 mm to 1 mm, which are referred as microchannel. This microfluidics is a multidisciplinary research area such as chemistry, biology, medicine, mechanical engineering, electrical and electronics engineering, physics, etc. The first microfluidic system was developed nearly in the mid-nineteenth century, which was used in the ink-jet print head. In recent years, microfluidic systems have found various applications like cell encapsulation, emulsification, chemical synthesis, drug formation and in lab-on-a-chip technology, etc. Microfluidic systems have many advantages such as it transfer small volume of fluid, takes less time for doing experiments, the cost of reagents are low, enhanced the performance, etc. For these advantages, many researchers focused on the design and development of microfluidic systems.

The microfluidic system may be a single phase system or multiphase system. In case of a single phase microfluidic system, single fluid flow in a microchannel and in case of multiphase microfluidic system two or more immiscible fluid flows in a microchannel. In multiphase microfluidic system mostly two-phase flow is considered. The two-phase flow in microchannel has many applications in the field of biomedical, micro-scale heat transfer, micro heat exchanger, lab-on-chip technology, microfiltration, micro-reactor, chemical synthesis, etc.

There are different types of two-phase flow present such as liquid-gas flows, liquid-liquid flow, liquid-solid flow, and gas-solid flow. Depending upon the geometries of microchannel, properties of the two fluids and flow rates of fluids, different types of flow regimes developed in the two-phase flow system, such as bubble flow, annular flow, churn flow and Taylor bubble flow.

Bubble flow occurs when small bubbles are suspended in a liquid continuum as a discrete particle. In case of annular flow, the liquid flows near the channel wall and the gas flows at the core of the channel. Churn flow is defined as the flow with the highly disturbed flow of liquid and gas. Taylor bubble flow is a gas-liquid flow regime which consisting of elongated bubbles and separated by liquid slugs. In this type of flow the elongation of the bubble is more than the hydraulic diameter of the channel.

From these different types of flow regimes, Taylor bubble flow in microchannel has major applications in micro reactor, removing heat in the micro heat exchanger and in other fields. For generating Taylor bubble flow different types of microchannel are used such as T-junction, Y-junction, annular and cross junction microchannel. In these types of the microchannel, two inlets are presents through which gas and liquid flows into the microchannel. The Taylor bubble flow is a best-desired flow regime for microbubble production in T-junction microchannel. Bubbles will form and flow when the gas (dispersed phase) enters at very low flow rate into a liquid (continuous phase) flowing channel. When the length of the bubble exceeds the channel diameter, then Taylor bubble generated.

An important category of multi-phase microfluidics is bubble/droplet-based microfluidics. In which discrete bubbles/droplets are generated and manipulated. In this type of microfluidic system, the dispersed phase fluid flows into the continuous phase fluid in a microchannel. When these two fluids brought into contact at a junction of channels, then the dispersed phase breaks into discrete

droplets/bubbles and transports downstream the channels in the surrounding of the continuous phase. In this bubble/droplet-based microfluidic system different types of operation can be obtained such as bubble/droplet generation, transporting, breakup, repartition, coalescence and so on. The bubbles and droplets can be controlled individually by considering them as individual micro reactors.

Different types of complex configuration are used for bubble/droplet microfluidic systems, such as T-junction divergence/convergence, loops, ladders, etc. T-junction divergence/ convergence have a wide range of application in droplet-based microfluidic systems in which many significant works like bubble/droplet formation, breakup, coalescence, etc. occur.

The bubble/droplet can be formed by using T-junction inlet in which continuous phase and dispersed phase flows perpendicular to each other and the bubble created at the T-junction. The bubble/droplet breakup can be obtained by doing some variations in the geometry of the microfluidic system. Mostly T-junction divergence used for the breakup process. For the bubble/droplet coalescence, T-junction divergence/convergence type configuration is used.

In recent years, T-junction divergence/convergence configuration is used for the breakup of bubble/droplet. The breakup of the bubble/droplet can be obtained in so many ways such as varying the geometry of the channel, by using some heating arrangements, by placing an obstacle in the channel, etc. The bubble/droplet breakup can be of three types, one is symmetrical breakup, second is asymmetrical breakup and third is no breakup. After the formation of bubble/droplet, the breakup occurs at the T-junction divergence. In a simple T-junction divergence (without any geometrical variation), the breakup process depends upon the inlet condition of the continuous phase fluid. By varying the inlet conditions, the above three bubble/droplet breakup process can be obtained. By using heat, the breakup process can be obtained. In this process, one branch of the

T-junction divergence got heated by using the heater. In this process, asymmetrical breakup occurs because the fluid in the heated branch is having lower viscosity, so the bigger daughter bubble moves towards that branch and the smaller daughter bubble move toward the unheated branch. After some temperature it may happen, instead of breaking off the bubble the single bubble moves to the heated branch, this process is known as bubble/droplet sorting. Another way by varying the geometry the breakup process can be obtained such as by varying the length of one of two branches of T-junction divergence, by varying width of one of two branches, by placing an obstacle at the T-junction divergence, by using valve in one branch of the T-junction divergence etc. In these process symmetrical and asymmetrical bubble/droplet breakup occurs. So many experimental and numerical works done so far in the microfluidic system, but the most focused area is the bubble/breakup process.

In this work the breakup of Taylor bubble obtained by using a microchannel having an upstream T-junction inlets and a downstream T-junction divergence where the obstacle is placed. Through the upstream T-junction air and water enters to the microchannel. Air is considered as dispersed phase, and water is considered as continuous phase. Initially the microchannel fill with water and air flow to the water flowing microchannel, due to which Taylor bubble created at the T-junction. After formation of the bubble the bubble breakup into two discrete daughter bubble at the T-junction divergence due to the presence of an obstacle. The breakup may be of symmetrical or asymmetrical depending upon the position of the obstacle at the T-junction divergence. A two dimension numerical simulation obtained by using commercially available ANSYS Fluent®.

Chapter-2

Literature Review

Several researchers experimentally and numerically studied the hydrodynamics of Taylor bubble flow in a microchannel. Study is also going on in the field of bubble/droplet-based microfluidic system that has a wide range of applications in recent years. Therefore microfluidic systems are prominent field of focus among leading researchers across the globe. The entire literature review comprises of two sections:

- Taylor bubble flow in the microchannel.
- Bubble/droplet based microfluidic systems.

2.1 Taylor bubble flow in microchannel:

Taylor bubble is defined as the liquid-gas flow regime that consists elongated bubble and separated by liquid slugs. Taylor bubble was predominantly found in microchannel where surface tension forces dominate the gravitational force. A century ago Gibson [1] was the first who studied the motion of air bubbles rising in a vertical tube. Later on due to the emergence of micro-manufacturing technology, many researchers studied the hydrodynamics of the Taylor bubble flow in microchannel.

Fairbrothers and Stubs [2] were experimentally studied the Taylor bubble flow in a vertical capillary tube. From this experiment, they found that a thin liquid film present in between the bubble and the wall of tube. Due to the presence of this liquid film the velocity of the bubble is more than that of the liquid.

Triplett et al. [3] studied experimentally the air-water two-phase flows through a circular microchannel, which has inner diameters of 1.1 and 1.45 mm and in a semi-triangular microchannel having hydraulic diameters of 1.09 and 1.49 mm. From this experiment, they obtained different flow patterns such as churn flow, bubbly flow, slug flow, and annular flow by varying the velocity of air and water.

Zhao et al. [4] experimentally studied the co-current upward air-water two-phase flow through a vertical triangular microchannel having a hydraulic diameter of 2.886, 1.443 and 0.866 mm. From this experiment different two-phase flow pattern such as slug flow, dispersed bubbly flow, annular flow, and churn flow are observed. They observed that when the channel diameter is 0.866 mm then dispersed bubbly flow was not found. From this experiment, capillary bubbly flow pattern was obtained.

Liu et al. [5] studied experimentally the hydrodynamics of two-phase flow in a vertical circular capillary tube of diameter 0.91, 2 and 3.02 mm and a vertical square capillary channel with hydraulic diameter of 0.99 and 2.89 mm. For this experiment, they took air as gas phase and water, ethanol and oil as liquid phase. From this experiment, they investigated the Taylor bubble flow pattern and the influence of liquid properties on Taylor bubble rise velocity.

Qian and Lawal [6] numerically studied the Taylor bubble flow in T-junction microchannel by varying the cross-sectional width (0.25, 0.5, 0.75, 1, 2 and 3 mm). From this simulation, they obtained different gas and liquid slug lengths by varying the inlet flow conditions and validate with the existing literature. Several correlations in the T-junction microchannel also find from this numerical work.

Santos and Kawaji [7] studied both experimentally, and numerically the gas-liquid two-phase flow in a T-junction microchannel having square cross-section with 1.33 μm hydraulic diameter.

They compare the results obtained from numerical simulation with the results obtained from experiments. Finally, they conclude that CFD codes can use to predict the Taylor bubble flow in the microchannel.

Zhang et al. [8] experimentally studied the influence of liquid physical properties and channel diameter on the gas-liquid two-phase flow in a horizontal circular microchannel. Three empirical correlations are proposed from this experiment for predicting the transitions from slug to churn flow and slug-annular flow, from slug to bubbly flow, and from churn to slug-annular and annular flow respectively.

Pham et al. [9] studied numerically the gas-liquid two-phase flow in T-junction microchannel in which they used volume-of-fluid method for simulation. From this simulation, they obtained the pressure, velocity distribution and phase of fluid in the microchannel.

Bretherton [10] experimentally studied the motion of long bubbles in a circular tube. From this experiment, some correlations for finding the thickness of the thin liquid film between the bubble and the tube wall are obtained.

Gupta et al. [11] studied numerically the Taylor bubble flow through a circular microchannel. From this simulation, they developed a method for capturing the thin liquid film that is present in between the Taylor bubble and the wall of the microchannel. They stated that for capturing liquid film fine mesh should be given near the wall. They also validated the result with previous experimental results.

Kang and Zhou [12] numerically studied the bubble generation and transport in a serpentine channel with T-junction inlet. For this simulation, they used multiphase three-dimensional Navier-stokes with volume-of-fluid method. From this, they studied the surface tension and viscosity effects on the generation of the bubble and validated it with experimental results.

Thippavathini and Moharana [13] numerically studied the flow of Taylor bubble in a microchannel in which an obstacle is present. The obstacle is used for creating turbulence due to which the heat transfer capacity increases. By varying the position of the obstacle in perpendicular direction the behavior of the Taylor bubble was observed.

Recently Dang et al. [14] numerically studied the formation of Taylor bubble in a microchannel in a converging shape mixing junction. In this simulation, they used two different interface capturing methods one is volume-of-fluid (VOF) method and other is coupled level set and VOF (CLSVOF). From this, the effects of contact angle, surface tension, and liquid viscosity on the Taylor bubble length, shape and volume are investigated.

From this literature reviews on Taylor bubble flow in microchannel, it is obtained that for numerical simulation the volume-of-fluid (VOF) method was frequently used. The Taylor bubble can be generated by flowing water and air in a T-junction microchannel with some appropriate velocity. The surface tension and contact angle should be given correctly. For capturing the liquid film near the wall, fine mesh will be required.

2.2 Bubble/droplet based microfluidic systems:

Microfluidics is defined as the science and technology of the system in which small volume of fluids can be controlled in a channel having a hydraulic diameter ranging between 0.001 mm to 1mm. This microfluidic device helps to generate bubbles/droplets of desirable sizes. The first microfluidics technology was developed in 1950 and used in today's ink-jet printer. In recent years, microfluidic systems have a wide range of applications in the fields of chemical, biomedical, micro-reactor, lab-on-chip technology, industrial, etc. So many researchers now give much attention to these microfluidic systems.

Thorsen et al. [15] experimentally studied the dynamic pattern formation in a vesicle-generating microfluidic device. In which they used oil (continuous phase) and water (dispersed phase) as working fluids. From this experiment, they conclude that the droplet generation is dominated by viscous effects and interfacial surface tension. They also observed that the droplet generation also depends upon the channel geometry and relative fluid pressure.

Stone et al. [16] gives the overview of flows in microfluidic devices and focused on different parameters like mixing, dispersion, bubble generation, transportation, controllability, and reproducibility, etc. They also highlighted some areas like, how the geometry of the microfluidic devices plays an important role, what is the driving force, what is the effect of surface tension, etc.

Tice et al. [17] described some experimental conditions required for the formation of nano-litre sized droplets of aqueous reagents which flows in an immiscible carrier fluid within a microchannel. They observed that the liquid plugs formed at lower capillary number (i.e. 0.01). They also described that the mixing of droplets in a straight microchannel can be enhanced by providing the combination of viscous and non-viscous reagents at ideal initial distribution.

Link et al. [18] proposed two methods for generating unequally sized droplets in a microfluidic device. In one method, they used T-junction with the unequal branch. From which they observed that after the breakup of droplets at T-junction, more bubble flows to the branch having smaller length. They defined that the bubble volume ratio between two branches was inversely proportional to the length ratio. However, disadvantage of this method is that by increasing or decreasing the branch length the manufacturing cost should be increased. In second method obstacle is used in the straight channel for the droplet breakup process. However, this method has disadvantage that after the breakup, small and large droplets are generates, then these droplets

move together along the channel and for again separation of these droplets another process is required.

Garstecki et al. [19] studied the formation and breakup of bubbles and droplets in a microfluidic T-junction. From this study, it was found that at very low capillary number, the bubble break-up process occurs due the pressure drop domination instead of the shear stresses domination. They also predict the size of bubbles and droplets produced in the T-junction at different flow rates, by varying geometrical dimensions, interfacial tension, etc.

Jousse et al. [20] studied both experimentally and numerically the bifurcation of droplet flows within capillaries. In which they used a simple channel that splits into two branches and subsequently recombine. From this different flow pattern, both periodic and irregular obtained which depends upon the frequency at which the droplet fed into the channel.

Ting et al. [21] studied both experimentally and numerically the droplet breakup process by using thermally induced surface tension gradient in a microchannel. A T-junction microchannel with one branch heated is used for the study. From this, they observed that after the breakup of the droplet at T-junction the larger size bubble flows to the heated branch due to the decrease in viscosity. After certain critical temperature, the droplet moves to the heated channel without breakup that is known as droplet sorting. However, the application of this method is limited.

Deremble and Tabeling [22] experimentally studied the droplet breakup process in microfluidic junction with arbitrary angles (Y-junction). From this, they found a critical length that controls the total breakup process. The experiments were done by taking small capillary numbers. However, this method has some disadvantages that are found in Link et al. [17].

Choi et al. [23] suggested a new method for producing asymmetrical droplets by using the pneumatic valve in the tube through which continuous fluid and droplets flows. When the droplet

passes through the pneumatic valve, then the droplet breaks into two unequal droplets based on the pneumatic valve pressure. This method has some disadvantages, after droplet breakup process both the smaller and larger droplets move along the channel, for again breakup another method is required. Another disadvantage is that for generating a specified droplet volume ratio, the pressure of the valve should keep constant. This because, the droplet volume ratio can change by a small change in pressure.

Zhu et al. [24] studied both experimentally and numerically the controllable breakup of droplets and bubble by using pneumatic valve. In this a pneumatic valve attached to the one branch of the T-junction with diverging and converging loop. By increase the pressure of the pneumatic valve the size of the bubble/droplet that moves to the branch with pneumatic valve is decreases. After some certain pressure of the pneumatic valve the bubble/droplet instead of breaking it moves to the branch without pneumatic valve. By varying pressure of the pneumatic valve, we can control the droplet/bubble size accordingly.

Bedram and Moosavi [25] numerically investigated the droplet breakup in asymmetric microfluidic T-junction, which consists of an inlet channel and two outlet channels with different width. From this simulation, it was observed that smaller size droplet moves to the channel with small width due to the flow resistance. They also observed that smaller droplets can be generated at the larger capillary number. In this method of droplet breakup, the breakup time and pressure drop are smaller than that of previously suggested methods for producing unequal size droplets.

Wu et al. [26] experimentally studied the asymmetrical breakup of bubbles in a microfluidic T-junction with divergence and convergence section. The channel has uniform square cross-section with 400 μm width and 400 μm depth. Gas and liquid used for generating bubble in the microfluidic channel. From this experiment four bubble behaviors are studied such as

asymmetrical collision of bubble pair, staggered flow of bubbles, the dynamic transformation of the bubble and single bubble flow. They also studied the feedback effects of the T-junction convergence on the bubble breakup at T-junction divergence. They observed that at lower flow rates the feedback effect of T-junction convergence is negligible, but at higher flow rate due to the collision of bubbles at T-junction convergence asymmetric bubble breakup occurs at the T-junction divergence.

Bedram and Moosavi [27] numerically studied the droplets breakup in micro and nanoscale T-junctions. For this simulation Volume of Fluid (VOF) method is used. They compared these numerical results with previously obtained experimental and analytical results. From this result, they found that, the breakup length and breakup time plays an important role in this systems. They also observed that in case of nanoscale T-junction the performance increases by increasing the capillary number but in case of micro-scale T-junction at a specific capillary number the system is in its optimum condition.

Hoang et al. [28] numerically studied the droplet breakup dynamics in a T-junction. In which three-dimensional T-junction microchannel is used. From this, they obtained two distinct breakup phases. The first phase in which the droplet deformation was driven by the externally applied flow, if the applied flow is stopped then the droplet come back to its original shape. Moreover, the second phase in which the droplet deformation driven by the surface tension which is independent of the externally applied flow, in this phase the droplet always breaks.

Bedram et al. [29] numerically investigated an efficient method for generating unequally sized droplets in Microfluidic and Nanofluidic systems. In this method, the breakup of droplets occurs by using a valve in one branch of the T-junction. For this numerical simulation Volume-of-Fluid, (VOF) method is used. From this, it was observed that smaller droplet moves to the branch with

valve. Also, the result shows that the breakup length does not vary with the valve ratio. By decreasing the capillary number the breakup length can be decreased in case of microscales, but in case of nanoscales the breakup length does not depend upon the capillary number. Another important parameter is found that the pressure drop decreases by increasing the valve ratio only when there are no tunnel forms, if the tunnel forms the pressure drop does not change with the valve ratio.

From these literature reviews, it was found that mostly the research were obtained to find different methods for bubble/droplet breakup in microfluidic systems. By using the concepts from the reviews presented above, a new method is used for the bubble breakup process, in which an obstacle is placed at the T-junction divergence. By varying the position and the height of the obstacle different parameters such as bubble length ratio, breakup time, breakup length and pressure drop are obtained.

Chapter-3

Numerical Simulation

3.1. Problem formulation:

In this work, a two-dimensional numerical simulation has been carried out to study the hydrodynamics of Taylor bubble breakup by placing an obstacle at the T-junction bifurcation.

In this study, a microchannel with an upstream T-junction and a downstream T-junction is used as shown in Fig. 3.1. Air (dispersed phase) and water (continuous phase) enters to the microchannel through the two inlets at the upstream T-junction and the Taylor bubble created at the T-junction. The obstacle is placed at the downstream T-junction, which helps to break the Taylor bubbles into two discrete Taylor bubbles having equal or unequal lengths depending upon the position of the obstacle. The microchannel having square cross-section with hydraulic diameter (D_h) of 0.2 mm and the length of the main channel is 4.5 mm. An obstacle of 0.01 mm thickness placed at the downstream T-junction bifurcation as shown in Fig 3.2. By varying the position and height of the obstacle different types of bubble breakup obtained such as symmetric breakup, asymmetric breakup and no breakup. The obstacle position varied from the center of the bifurcated T-junction to the right side branch (i.e. X = 0, 0.025, 0.05, 0.075 and 0.1 mm) and the height varied as (Y = 0.05, 0.1, 0.15 and 0.2 mm). Initially, water is present inside the main channel, and the air enter into the main channel through the inlet of the upstream T-junction. The air and water flow into the channel by assuming as laminar flow at the inlets. The water velocity at the inlet is set to 0.251 m/s according to the Re = 50 and the air velocity at the inlet is set to 0.154 m/s according to the

Re = 2. Different cases are done by varying height and position of the obstacle. Some parameters like bubble length ratio, bubble breakup length, bubble breakup time and pressure drop at the time of bubble breakup are studied in different cases, and some plots are obtained.

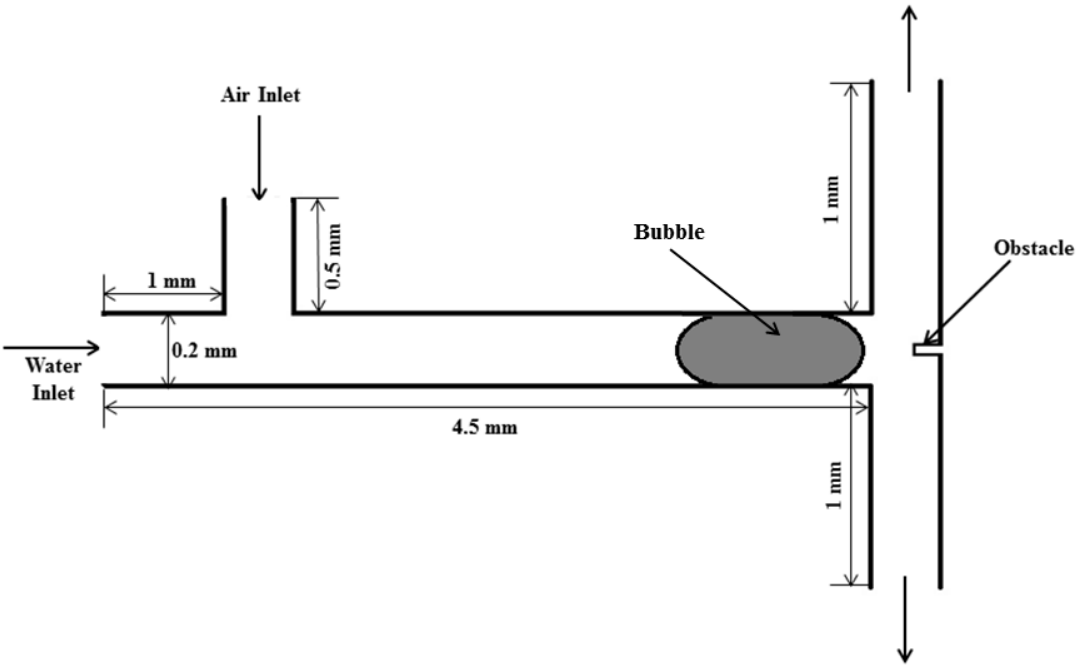

Fig. 3.1. Top view of T-junction microchannel with bifurcation.

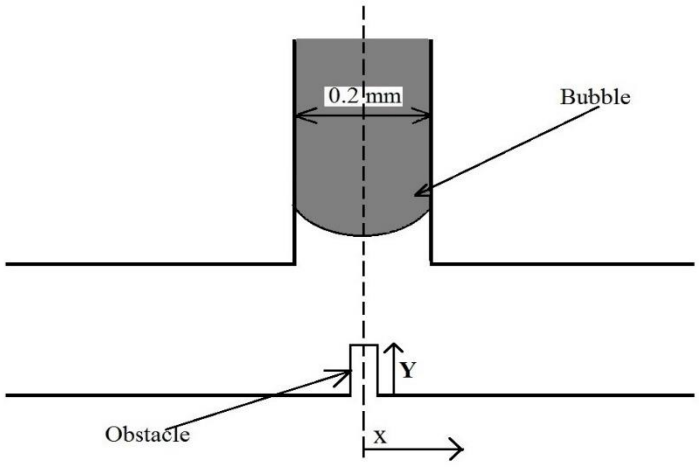

Fig. 3.2. The T-junction bifurcation showing the position of the obstacle.

3.2. Governing equations:

In this work, the numerical simulation of the multiphase flow of air and water in T-junction microchannel is obtained by using Volume of Fluid (VOF) multiphase model that is available in ANSYS Fluent® software. The VOF model is used to compute the volume fraction and helps to track the interface between two immiscible fluids. The governing equations are given below.

Continuity equation:

$$\frac{\partial \rho}{\partial t} + \nabla.(\rho \vec{v}) = 0 \tag{1}$$

Navier-Stokes equation:

$$\frac{\partial (\rho \vec{v})}{\partial t} + \nabla.(\rho \vec{v}\vec{v}) = -\nabla p + \nabla.[\mu(\nabla \vec{v} + \nabla \vec{v}^{T})] + \vec{F} \tag{2}$$

where t is time, p is pressure, ρ is density, $\vec{v}$ is velocity vector, μ is the dynamic viscosity of the fluid and $\vec{F}$ is surface tension force of the fluid. T is transpose.

Volume fraction equation:

$$\frac{\partial \alpha}{\partial t} + \vec{v}.\nabla \alpha = 0 \tag{3}$$

$$\rho = \alpha_G \rho_G + (1 - \alpha_G)\rho_L \tag{4}$$

$$\mu = \alpha_G \mu_G + (1 - \alpha_G)\mu_L \tag{5}$$

where α is the volume fraction of the fluid, ρ is density and μ are the dynamic viscosity of the fluid. G and L are the subscript for gas (air) and liquid (water) respectively.

Dimensionless numbers:

Some dimensionless numbers plays crucial role in the fluid flow such as Reynolds number, Capillary number, Weber number, Froude number, Bond number, etc. In this work Reynolds number (Re) and Capillary number (Ca) are considered.

Reynolds number is defined as the ration between inertia force and viscous force. The fluid flow in a channel or tube is said to be laminar when Re > 2000 and turbulent when Re > 4000. The Reynolds number defined mathematically as below:

$$Re = \frac{\rho v D_h}{\mu} \tag{6}$$

where v is the velocity of the fluid, ρ is the density and μ are the dynamic viscosity of the fluid, D_h is the hydraulic diameter of the channel.

The hydraulic diameter of a circular tube is the diameter of the tube. For the channel or duct having rectangular cross-section the hydraulic diameter is found by using the below formula:

$$D_h = \frac{4A}{P} \tag{7}$$

where A is, the cross-sectional area of the duct and P is the perimeter of the duct.

The capillary number is a dimensionless number that gives the relation between the viscous force and the surface tension force. For low capillary numbers ($Ca < 10^{-5}$) surface tension force dominates the viscous force due to which the bubbles generates in the microchannel. When the capillary number is more ($Ca > 10^{-5}$) the viscous force dominates the surface tension force that leads to the annular flow. The capillary number is defined as:

$$Ca = \frac{\mu_L (v_L + v_G)}{\sigma} \tag{8}$$

where μ is the dynamic viscosity, v is the velocity and σ is the coefficient of surface tension between liquid and gas. L and G are the subscripts for the liquid and gas respectively [11].

Bretherton [10] proposed a correlation between the liquid film thickness (δ) and the Capillary number (Ca), which is given below:

$$\delta = 1.34 R.Ca^{\frac{2}{3}} \tag{9}$$

where R is the radius of the channel.

Gupta et al. [11] stated in his work that for capturing the liquid film thickness present in between the channel wall and the Taylor bubble numerically, the mesh should be very fine near the wall. That means nearly five to seven grids are present inside the liquid film thickness (δ). Due to the presence of this liquid film thickness the velocity of the dispersed phase (bubble) is more. This liquid film surrounded the bubble due to which the bubble cannot make contact with the channel wall.

Another important number is the Courant number (C), which helps in solving certain partial differential equations numerically. This number is described by three mathematician Richard Courant, Kurt Friedrichs and Hans Lewy, so the condition is also known as Courant-Friedrichs-Lewy (CFL) condition. The Courant number is defined as below:

$$C = \Delta t \sum_{i=1}^{n} \frac{u_{x_i}}{\Delta x_i} \tag{10}$$

where u is the velocity magnitude, Δx is the length interval, Δt is the time step size, i indicate the node number and n indicate the total number of nodes.

3.3. CFD modelling:

The complete numerical simulation is obtained by using the commercial ANSYS Fluent® version 15. This simulation is having four stages such as geometry creation, meshing, setup and solution in Fluent®. These stages are described below.

3.3.1. Geometry creation:

The computational domain geometry was created in ANSYS Workbench. The geometry considered in this work having a loop at the downstream T-junction with diverging and converging section (Fig. 3.3). However, the focused area is the T-junction bifurcation where the obstacle is present. So all the data analyzed at that portion only. The microchannel having the square section with a hydraulic diameter of 0.2 mm and the length is 4.5 mm. The auxiliary channel at the

upstream T-junction is having 0.5 mm length. There is a loop formed at the upstream T-junction with diverging and converging section. An obstacle of thickness 0.01 mm placed at the T-junction bifurcation. For creating the geometry in ANSYS Workbench, Fluid flow (Fluent) was selected from the toolbox. Then DESIGN MODELER was opened in which geometry was created. In the analysis type 2D must be selected in place of 3D. In DESIGN MODELER, mm is selected as the unit and XY-plane selected for the sketching of geometry. By drawing some length as per the given dimension, the complete sketch was completed. Then the surface created from this sketch by clicking on concept-surface from sketches. Then the surface body was defined as fluid. After that, the geometry was saved.

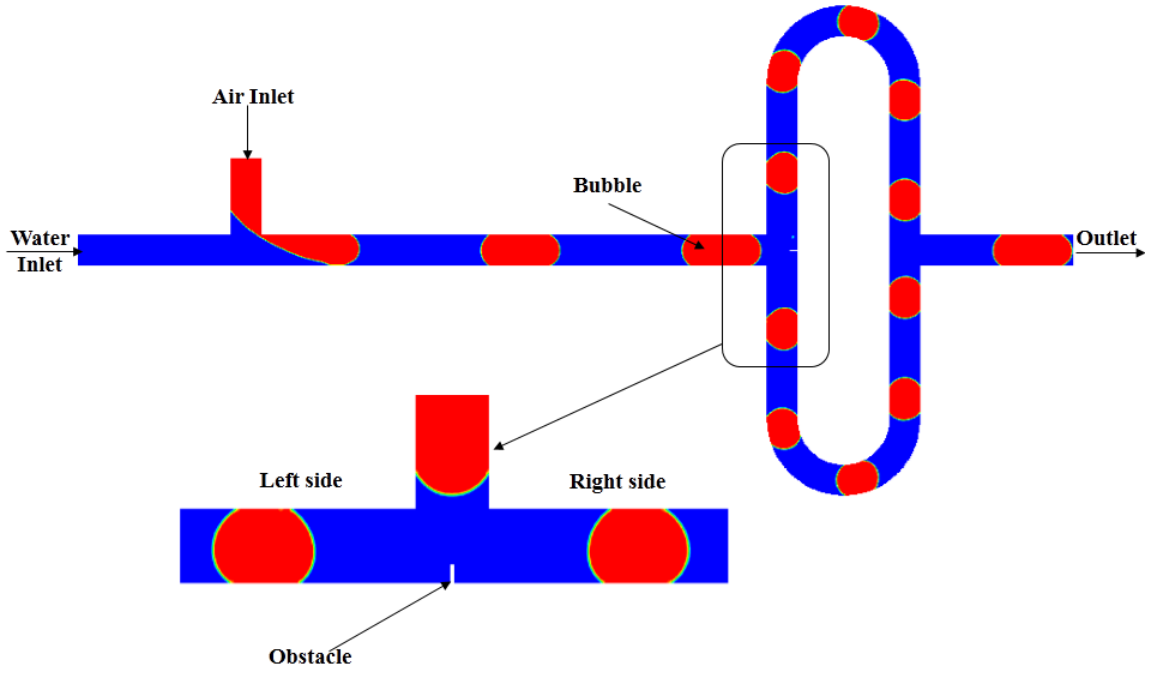

Fig. 3.3. Geometry of the T-junction microchannel with loop.

3.3.2. Meshing:

Mesh size play crucial role in the outcome of the numerical simulation. So for the accuracy of the simulation, fine mesh is always desirable. After completion of the geometry, mesh was selected on the workbench. A new window opened where the mesh will be generated. By clicking on

generate mesh the mesh generates, but it obtained by taking the by default values. The mesh can be generated accordingly by using different options available in mesh control. In mesh control, first meshing method was selected in which quad was selected as meshing method. After that face mapping was done by using mapped facing in which all the faces are selected. Then edge sizing was done in which the edges are selected, no of division was given on each edge and the grid type was selected as hard. After these steps, the mesh was generated. For this geometry, the edge sizing was chosen as 0.005 mm for generating structure grid (see Fig. 3.4). For obtaining this edge sizing, grid independence test was done which is described in next section. After mesh generation naming of different edges was done by selecting the edges and create named selection. Then mesh was exported to use in Fluent®.

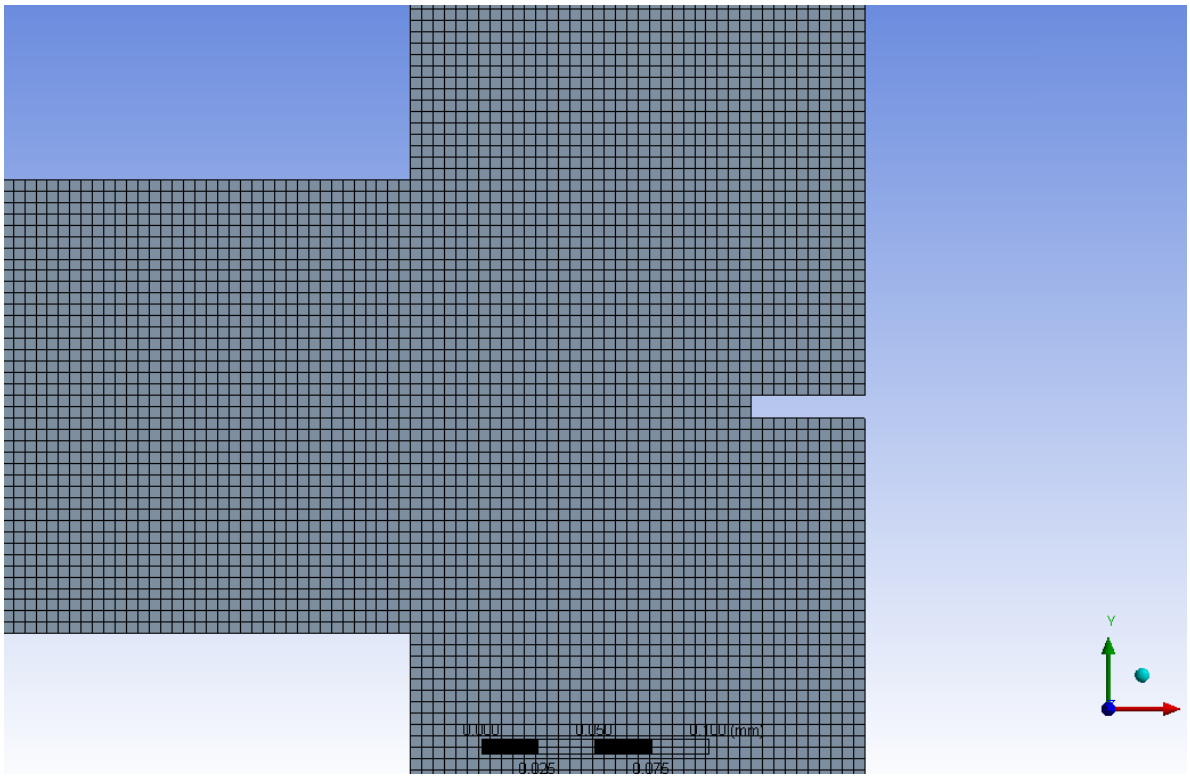

Fig. 3.4. Grids of the computational domain.

3.3.2.1. Grid independence test:

For obtaining best grid size for meshing, grid independence test was done. In this work the grid independence test was carried out by taking four no. of edge sizing, such as 0.01 mm, 0.008 mm, 0.005 mm and 0.004 mm. By using these edge sizing in this geometry, grid generation occurs. After complete the solution, contours of the volume fraction of air just before the bubble breakup is captured for different edge sizing. Then the grid independence test result obtained by calculating the bubble length, as shown in Fig. 3.5.

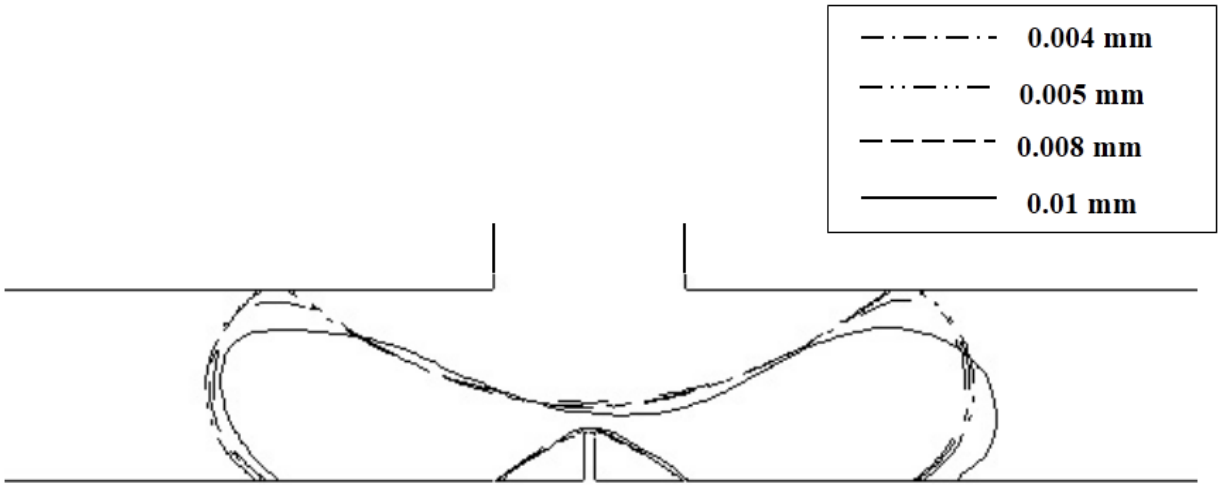

Fig. 3.5. Grid independence test result.

From this, it is observed that for the grid size 0.01 mm the shape and size of the bubble is not good. For grid size 0.008 mm the bubble shape and size is better than that of for 0.01 grid size. However, for the grid size of 0.005 mm and 0.004 mm, the shape and size of the bubble is same and obtained a perfect shape. So for this problem the grid size of 0.005 mm was chosen for the grid generation purpose. The grid size of 0.004 mm was not chosen because, for this grid size the no. of elements is more which takes more time for simulation. So for consuming less time and for obtaining good results the grid size of 0.005 mm was taken.

3.3.3. Setup in Fluent®:

The numerical simulation of fluid flow is solved by using the commercial software ANSYS Fluent®. Prior to the simulation in Fluent® the mesh generation of the computational domain must be completed. When Fluent® opened there is an option for choosing 2D or 3D analysis type if it was not selected at the time of geometry creation. After opening of Fluent® the exported mesh was read. First of all the mesh was checked whether the aspect ratio is good or not, whether the orthogonal quality was nearly equal to one, etc. In the general menu of the setup pressure-based type, absolute velocity formulation, transient time and planar 2D space selected for the solver. There was no role of gravity in this problem, so gravity was not selected.

In the model menu, the multiphase model was selected because it is a multiphase flow simulation. There are mainly three types of multiphase models present in the Fluent® such as Volume-of-Fluid (VOF) model, Mixture model, and Eulerian model. From these models, the VOF model mostly used to capture the interface between two or more immiscible fluids. In this work VOF model used as the multiphase model and explicit scheme used as the volume fraction parameters. Energy tab was remained off because it is a purely fluid flow problem. Laminar flow was chosen as viscous. Water and air were taken as the working fluids in material selection. The thermos-physical properties of air and water are given in the table 3.1.

Table 3.1. Thermo-physical properties of water and air

Property	**Symbol**	**Air**	**Water**	**Unit**
Density	ρ	1.225	998.2	kg/m^3
Dynamic viscosity	μ	1.79e-5	0.00103	kg/m-s
Specific heat at constant pressure	C_p	1006.43	4182	J/kg-K
Thermal conductivity	k_f	0.0242	0.6	W/m-K

In phase, menu air was selected as primary phase and water were selected as secondary phase. Initially the secondary phase (water) was present in the channel, and the primary phase (air) enter into the channel through air inlet. Surface tension force modeling selected in the phase interaction menu, in which continuum surface force (CSF) model was chosen, and wall adhesion also selected. The surface tension coefficient between water and the air was taken as 0.0735 N/m [9]. The contact angle for water and air with the wall was taken as 36º.

Then the boundary condition were given. The inlet velocity for water was taken as 0.251 m/s and for air as 0.154 m/s according to Re = 50 and Re = 2 respectively. The multiphase volume fraction for water and air were chosen as one and zero respectively. The volume fraction one means the channel initially filled with water. All the walls were insulated, and outlet was selected as pressure-outlet. After completion of the Fluent® setup, the next step is to go for the solution.

3.3.4. Solution:

In solution menu for pressure-velocity coupling 'PISO' scheme was used, 'Green-Gauss cell-based' theorem used for gradient computation, for pressure discretization 'PRESTO' scheme was used, for momentum discretization 'second order upwind' scheme was used and for the discretization of volume fraction 'geo-reconstruct' scheme was used. In residual monitors, convergence criteria were set as 10^{-6} for continuity, x-velocity and y-velocity residuals. Standard initialization was done by computing from the water inlet. After initialize the case and data file was saved.

In run calculation menu variable time-stepping method was chosen and in which the global Courant number was set as 0.25, the ending time taken as 1000 s, the minimum and maximum time step size considered as 10^{-8} and 10^{-4} respectively, and all remaining values were set as default value. The number of time steps was set as 10^{6} and maximum iteration per time step set as 20.

Then the calculation runs. After the calculation completes, the contours of the volume fraction of air at different time steps are extracted, and some lines are created in the domain for the calculation of pressure at a different position. Different parameters are defined and calculated which are discussed in the next chapter.

Chapter-4

Result and Discussion

In this chapter, the results of Taylor bubble breakup in a T-junction microchannel with an obstacle at the T-junction bifurcation are given. Fig. 3.1 describes the geometry of the microchannel with an upstream T-junction and a downstream T-junction bifurcation. An obstacle is placed at the T-junction bifurcation for the breakup process. The width of the obstacle taken as 0.01 mm. Water and air enters to the microchannel through the inlets of upstream T-junction with a velocity of 0.251 m/s (Re = 50) and 0.154 m/s (Re = 2). When air enters into the water flowing microchannel, then the Taylor bubble forms at the upstream T-junction. The bubble length is greater than the hydraulic diameter of the microchannel, so it is also known as elongated bubble. After the formation of Taylor bubble at the upstream T-junction, the breakup process takes place at the downstream T-junction bifurcation. Different types of bubble breakup such as symmetrical breakup, asymmetrical breakup and no breakup are studied by varying the obstacle position and height in x and y directions respectively.

In this work different cases are studied by varying the obstacle position and height alternatively i.e. by keeping constant the height of the obstacle, position varied and vice versa. From these cases, we studied different parameters like, Taylor bubble formation at upstream T-junction, bubble breakup at downstream T-junction bifurcation, bubble length ratio, bubble breakup length, bubble breakup time and pressure drop. The contours of the volume fraction of air at different time step for the different cases are also given. Finally, different plots are also obtained.

4.1. Taylor bubble formation:

Fig. 4.1 shows the process of Taylor bubble formation in the T-junction. Two immiscible fluid (air and water) enter to the microchannel through the inlets of upstream T-junction and forms an interface at the junction. In this figure, the contours of volume fraction of air are shown. Where the red color indicates air, and the blue color indicates water. When the dispersed phase (air) penetrates into the continuous phase (water) flow in the main channel, a bubble formed and begins to grow towards the main channel, as seen in Fig. 4.1 (a-b). Due to the pressure gradient and water flows in the main channel the bubble get distorted and try to flow in the downstream direction as seen in Fig. 4.1 (c). As time increases, the bubble elongates, and the tip of the bubble moves towards the downstream direction, as seen in Fig. 4.1 (d). The neck, which connects the air inlet channel with the bubble get thinner as time increases, as seen in Fig 4.1 (e). After some time, the neck breaks and the bubble flow in a downstream direction in the main channel, as seen in Fig. 4.1 (f-h). By this process, the Taylor bubble formation occurs at the upstream T-junction. After formation of one bubble, the tip of the dispersed phase (air) retain at the end of the inlet of T-junction and the same process repeats.

From the Fig. 4.1 (h), it was seen that a thin liquid film thickness formed between the bubble and the channel wall. Due to this film thickness the velocity of the bubble is more than that of the continuous phase (water). From this, it was also observed that the length of the bubble is more than the diameter of the channel. The length of the bubble can be varied by varying the inlet parameters. If the velocity of water increases and air velocity keep constant, smaller length bubbles are formed. Similarly, by keeping water velocity constant and increasing the air velocity, larger length bubbles are formed. After formation of the Taylor bubble, the breakup processes at the T-junction bifurcation are discussed in the next section.

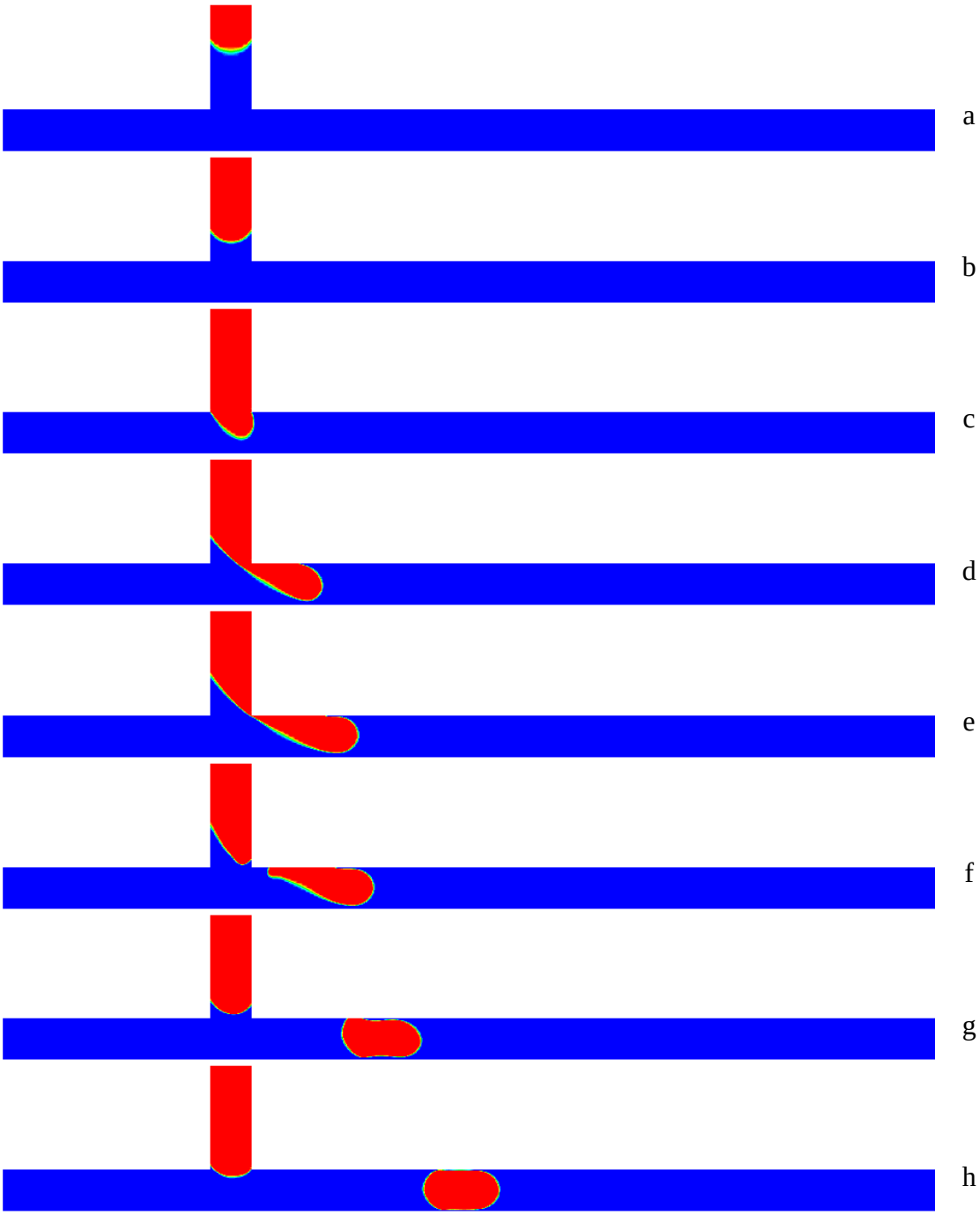

Fig. 4.1. Taylor bubble formation at the upstream T-junction.

4.2. Taylor bubble breakup process without obstacle:

In this case, there is no obstacle present at the downstream T-junction bifurcation. The Taylor bubble flow towards the downstream T-junction bifurcation at which the breakup of the bubble will occur. In this case, the bubble breakup occurs due to the shape of the geometry and the flow condition. The image sequence of complete Taylor bubble breakup process is shown in Fig. 4.2. As there is no obstacle present at the T-junction bifurcation, the water flow into both the branches at same flow rates. Before entering into the T-junction, the Taylor bubble is symmetrical in shape, as shown in Fig. 4.2 (a). When it enters into the T-junction, the shape of the bubble starts changing, as shown in Fig. 4.2 (b). After some time, the front meniscus touches the wall of the T-junction, and the bubble starts advancing towards both the branches, as shown in Fig. 4.2 (c-e). The length of the bubble increases as time increases, and the middle part of the bubble get thinner, as shown in Fig. 4.2 (f-g). After reaching a maximum length, which is known as bubble breakup length, the bubble breaks into two discrete daughter bubbles, as shown in Fig. 4.2 (h-j). These daughter bubbles start move towards both the branches of the T-junction in the opposite direction. After some time, both the daughter bubbles obtained the shape similar to that of the parent bubble, as shown in Fig. 4.2 (k-l). In this way the Taylor bubble breakup process occurs.

In this case, it is found that, both the daughter bubbles are of the same length, so it is a symmetrical breakup process, as shown in Fig. 4.2 (m). Same process obtained for all the Taylor bubbles that are come from the upstream T-junction towards the downstream T-junction bifurcation. For obtaining, unequal daughter bubbles, an obstacle is to be positioned at the T-junction bifurcation. By varying the position of the obstacle unequal bubbles, can be obtained. So in this work an obstacle is positioned at T-junction bifurcation for obtaining the asymmetrical breakup of the bubble.

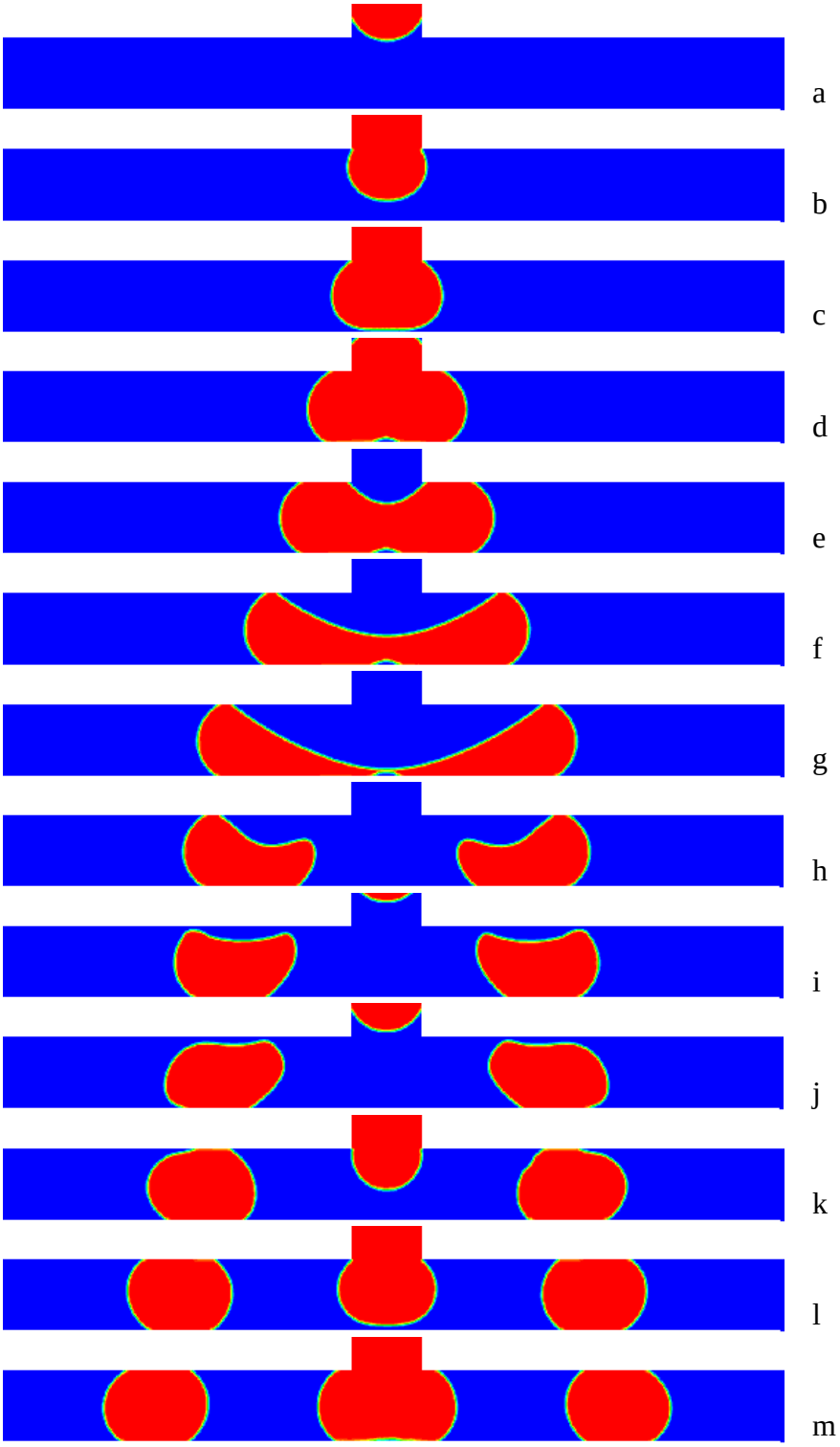

Fig. 4.3. Taylor bubble breakup process, without obstacle.

4.3. Taylor bubble breakup process by using obstacle:

In this case, an obstacle is positioned at the center of the T-junction bifurcation. When the tip of the bubble touches this obstacle, then it breaks into two discrete daughter bubbles. This breakup process may be of symmetrical or asymmetrical depending upon the position of the obstacle. In this work, different cases are studied by varying the position of the obstacle and keeping constant the height and vice versa.

4.3.1. Varying obstacle position with constant height:

In this case, the height of the obstacle keep constant and the position is varied. For this the height of the obstacle taken as Y = 0.05 mm, that is one-fourth of the width of the microchannel. And the position is varied towards the right side branch as X = 0, 0.025, 0.05, 0.075 and 0.1 mm.

4.3.1.1. Obstacle positioned at X = 0 mm:

In this case, the obstacle is positioned at X = 0 mm, i.e. at the center of the T-junction bifurcation. The sequence of the images showing the breakup process of the Taylor bubble at different time step is presented in Fig. 4.3. The Taylor bubble is symmetric in shape before entering into the T-junction, as shown in Fig. 4.3 (a-b). At first the front meniscus of the Taylor bubble touches the obstacle as it is placed at the center of the T-junction bifurcation. When the Taylor bubble touches the obstacle, it expanded towards both the branches of the T-junction and started advancing opposite to each other, as shown in Fig. 4.3 (c-e). Due to this the bubble length increases with respect to time, and also the middle part of the bubble get thinner, as shown in Fig. 4.3 (f-h). After reaching its maximum length, which is known as the bubble breakup length, the bubble breaks into two separate daughter bubbles, as shown in Fig. 4.3 (i-m). From Fig. 4.3 (m) it is found that, both the daughter bubbles are of same length. In this case the symmetrical breakup process occurs, because the obstacle positioned exactly at the center of the bifurcation.

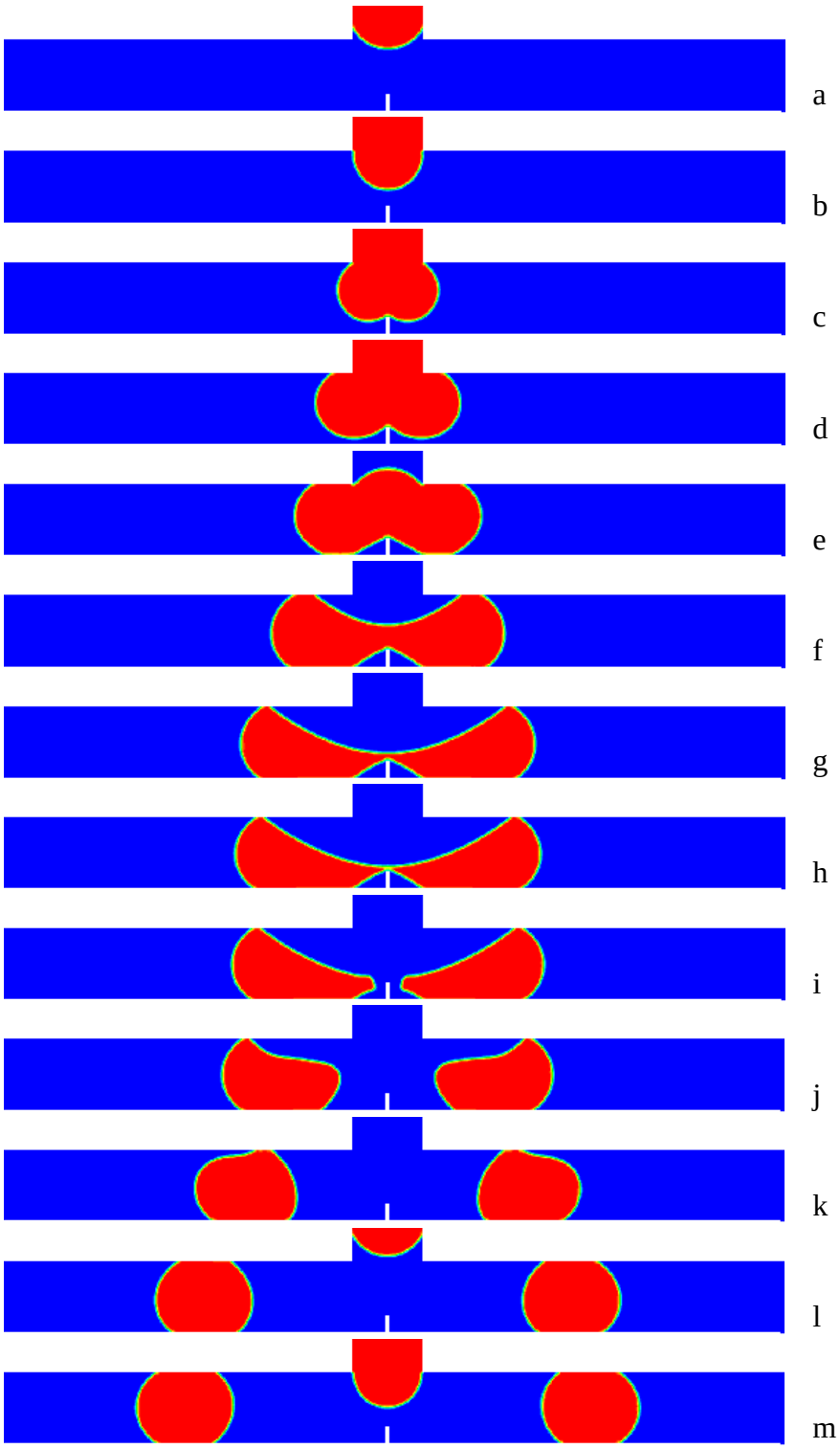

Fig. 4.3. Taylor bubble breakup process, when the obstacle positioned at X = 0 mm (center)

4.3.1.2. Obstacle positioned at X = 0.025 mm:

In this case, the obstacle is shifted to 0.025 mm right of the center of the T-junction bifurcation. Fig. 4.4 represents the image sequence of the Taylor bubble breakup process for this case. Before entering into the T-junction, the Taylor bubble is in symmetrical shape, as shown in Fig. 4.4 (a). When it enters into the T-junction and touches the obstacle, the bubble shape changes. As the obstacle positioned to the right of the center, the front meniscus first touches the tip of the obstacle on its right, as shown in Fig. 4.4 (b-c). After touching the obstacle the bubble started to move towards both the branches of the T-junction and developed two independent meniscus, as shown in Fig. 4.4 (c). Due to this type of obstacle positioning, the resistance to flow is more in the right side branch of the bifurcated T-junction. So small meniscus develops on the right side, and large meniscus develops on the left side of the obstacle, and both the meniscus starts moving forward in opposite to each other, as shown in Fig. 4.4 (d-e). Due to this the bubble length extended as time increases and the middle part of the bubble get thinner, as shown in Fig. 4.4 (f-i). After extended to its maximum length, which is known as bubble breakup length, the bubble breaks into two discrete daughter bubbles, as shown in Fig. 4.4 (j). After the breakup occurs, both the bubble starts to move into both the branches of the T-junction opposite to each other, as shown in Fig. 4.4 (k-l). After some time, both the daughter bubbles obtained the shape similar to that of the parent bubble, as shown in Fig. 4.4 (m). In this way the Taylor bubble breakup occurs for this case.

In this case, it is found that the length of the right side bubble is less than that of left side bubble, as shown in Fig. 4.4 (m). So it is an asymmetrical breakup process. It is also found that the bubble breakup length is more than that obtained in the previous cases. Same process obtained for all the Taylor bubbles that are come from the upstream T-junction towards the downstream T-junction bifurcation.

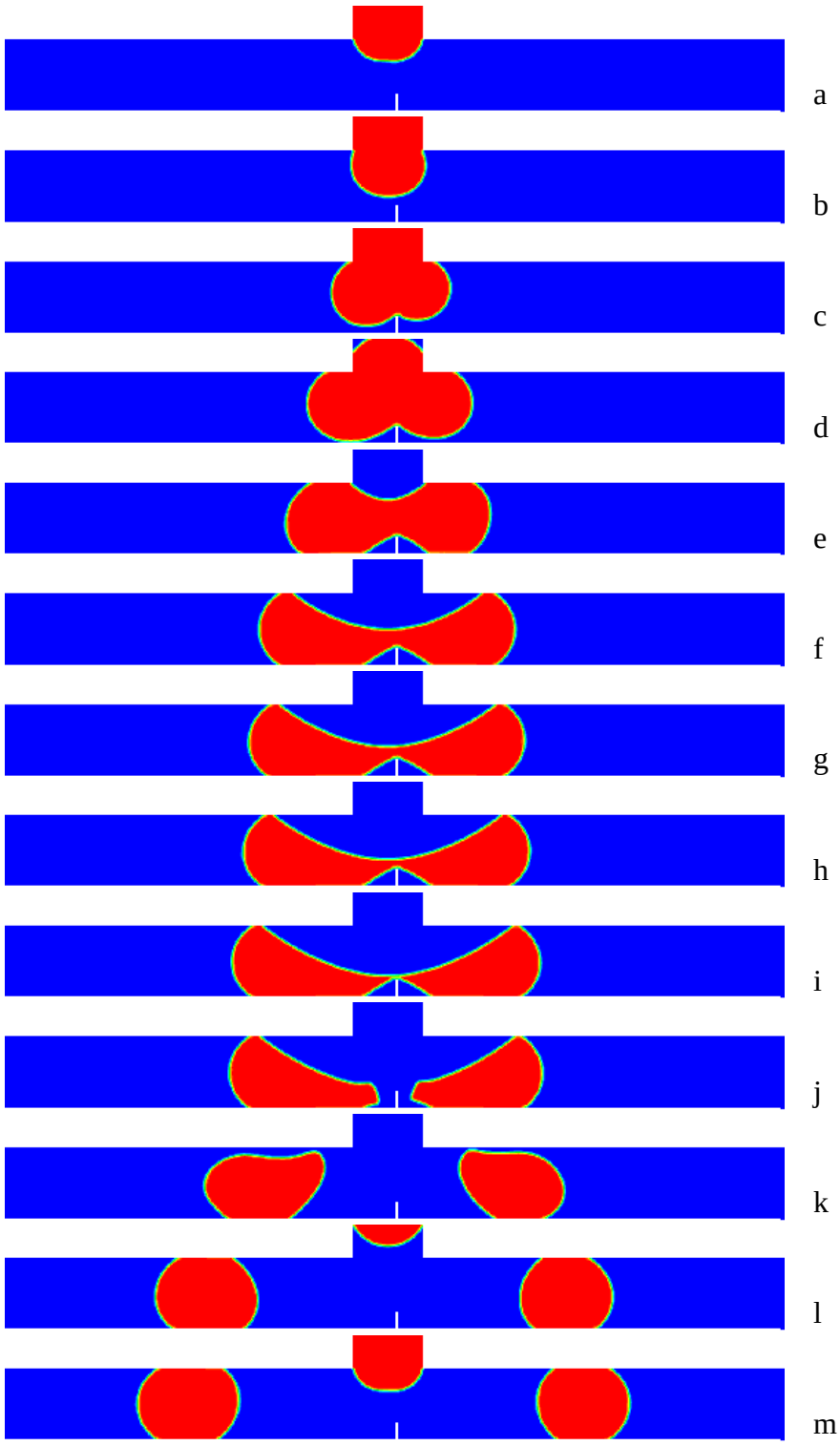

Fig. 4.4. Taylor bubble breakup process, when the obstacle positioned at X = 0.025 mm.

4.3.1.3. Obstacle positioned at X = 0.05 mm:

In this case, the obstacle shifted to 0.05 mm right of the center of the T-junction bifurcation. The image sequence of complete Taylor bubble breakup process is shown in Fig. 4.5. Before entering into the T-junction, the Taylor bubble is in symmetrical shape, as shown in Fig 4.5 (a). When the bubble enters into the T-junction, the shape of the bubble changes. As the obstacle positioned to the right of the center, the front meniscus first touches the tip of the obstacle on its right, as shown in Fig. 4.5 (b-c). After touching the obstacle the bubble started to move towards both the branches of the T-junction and developed two independent meniscus, as shown in Fig. 4.5 (c). Due to this type of obstacle positioning, the resistance to flow is more in the right side branch of the bifurcated T-junction. So small meniscus develops on the right side and large meniscus develops on the left side of the obstacle, and both the meniscus starts moving forward in opposite to each other, as shown in Fig 4.5 (d-e). Due to this the bubble length extended as time increases and the middle part of the bubble get thinner, as shown in Fig. 4.5 (f-h). After extended to its maximum length, which is known as bubble breakup length, the bubble breaks into two discrete daughter bubbles, as shown in Fig. 4.5 (i). After the breakup occurs, both the daughter bubble starts to move into both the branches of the T-junction opposite to each other, as shown in Fig. 4.5 (j-l). After some time, both the daughter bubbles obtained the shape similar to that of the parent bubble, as shown in Fig. 4.5 (m). In this way the Taylor bubble breakup occurs for this case.

In this case, it is found that the length of the right side bubble is less than that of left side bubble, as shown in Fig. 4.5 (m). So it is an asymmetrical breakup process. It is also found that the bubble breakup length is more than that obtained in the previous cases. Same process obtained for all the Taylor bubbles that are come from the upstream T-junction towards the downstream T-junction bifurcation.

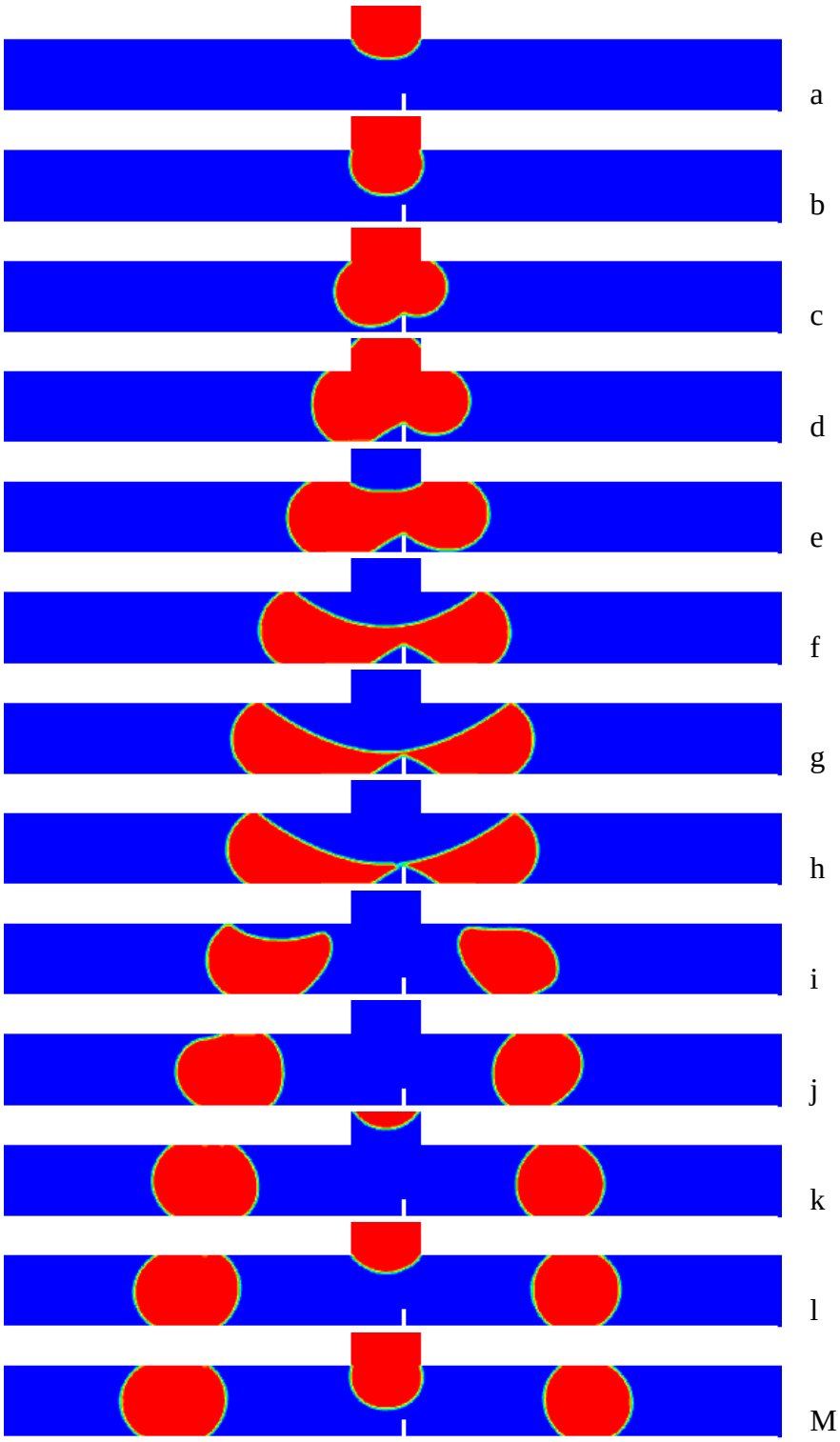

Fig. 4.5. Taylor bubble breakup process, when the obstacle positioned at X = 0.05 mm.

4.3.1.4. Obstacle positioned at X = 0.075 mm:

In this case, the obstacle shifted to 0.075 mm right of the center of the T-junction bifurcation. The image sequence of complete Taylor bubble breakup process is shown in Fig. 4.6. Before entering into the T-junction, the Taylor bubble is in symmetrical shape, as shown in Fig 4.6 (a). When the bubble enters into the T-junction, the shape of the bubble changes. As the obstacle positioned to the right of the center, the front meniscus first touches the tip of the obstacle on its right, as shown in Fig. 4.6 (b-c). After touching the obstacle the bubble started to move towards both the branches of the T-junction and developed two independent meniscus, as shown in Fig 4.6 (c). Due to this type of obstacle positioning, the resistance to flow is more in the right side branch of the bifurcated T-junction. So small meniscus develops on the right side and large meniscus develops on the left side of the obstacle, and both the meniscus starts moving forward in opposite to each other, as shown in Fig 4.6 (d-e). Due to this the bubble length extended as time increases and the middle part of the bubble get thinner, as shown in Fig. 4.6 (f-h). After extended to its maximum length, which is known as bubble breakup length, the bubble breaks into two discrete daughter bubbles, as shown in Fig. 4.6 (i). After the breakup occurs, both the daughter bubble starts to move into both the branches of the T-junction opposite to each other, as shown in Fig. 4.6 (j-l). After some time, both the daughter bubbles obtained the shape similar to that of the parent bubble, as shown in Fig. 4.6 (m). In this way, the Taylor bubble breakup occurs for this case.

In this case, it is found that the length of the right side bubble is less than that of left side bubble, as shown in Fig. 4.6 (m). So it is an asymmetrical breakup process. It is also found that the bubble breakup length is more than that obtained in the previous cases. Same process obtained for all the Taylor bubbles that are come from the upstream T-junction towards the downstream T-junction bifurcation.

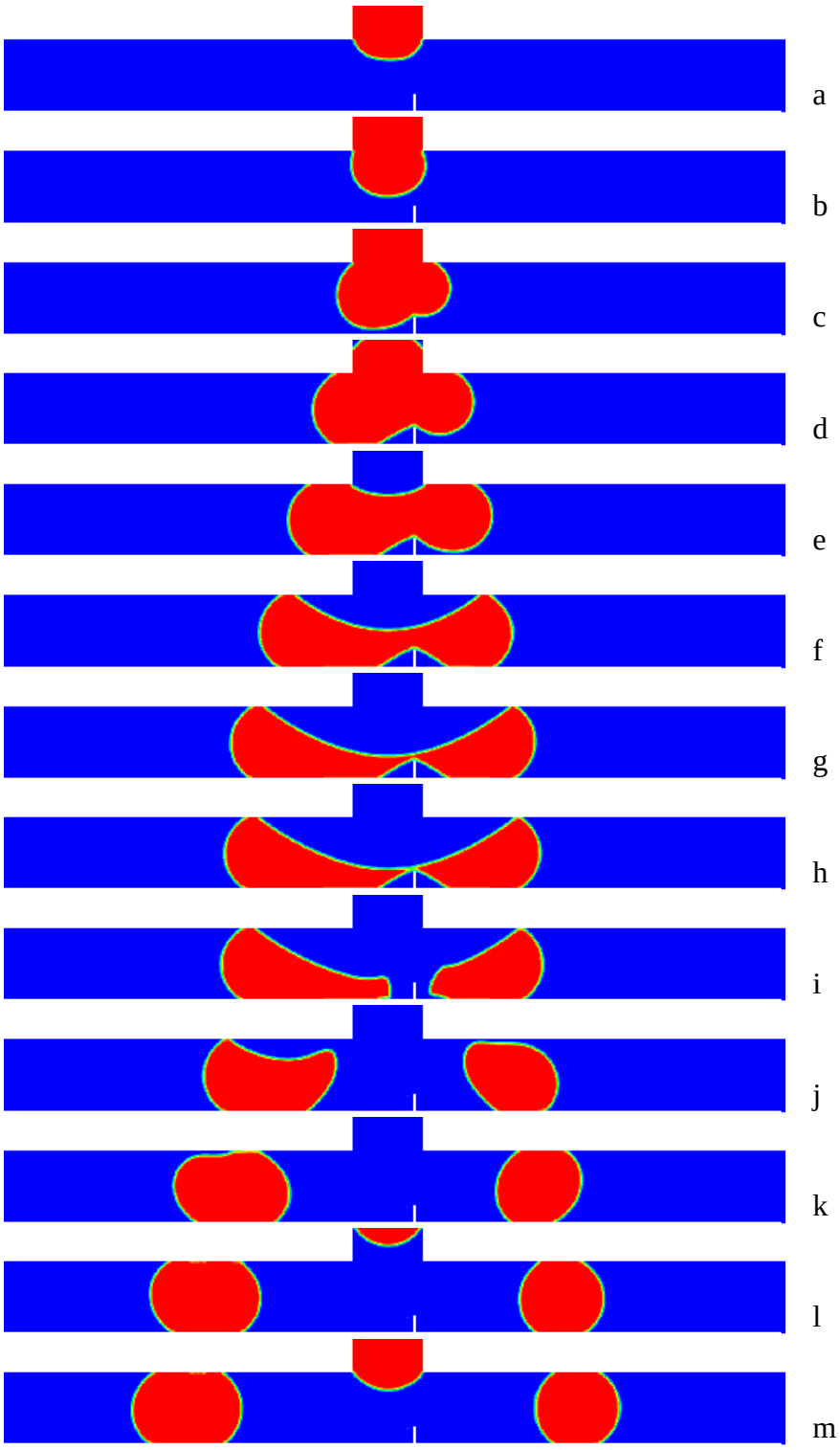

Fig. 4.6. Taylor bubble breakup process, when the obstacle positioned at X = 0.075 mm.

4.3.1.5. Obstacle positioned at X = 0.1 mm:

In this case, the obstacle shifted to 0.1 mm right of the center of the T-junction bifurcation. The image sequence of complete Taylor bubble breakup process is shown in Fig. 4.7. Before entering into the T-junction, the Taylor bubble is in symmetrical shape, as shown in Fig 4.7 (a). When the bubble enters into the T-junction, the shape of the bubble changes. As the obstacle positioned to the right of the center, the front meniscus first touches the tip of the obstacle on its right, as shown in Fig. 4.7 (b-c). After touching the obstacle the bubble started to move towards both the branches of the T-junction and developed two independent meniscus, as shown in Fig 4.7 (c). Due to this type of obstacle positioning, the resistance to flow is more in the right side branch of the bifurcated T-junction. So small meniscus develops on the right side and large meniscus develops on the left side of the obstacle, and both the meniscus starts moving forward in opposite to each other, as shown in Fig 4.7 (d-e). Due to this the bubble length extended as time increases and the middle part of the bubble get thinner, as shown in Fig. 4.7 (f-h). After extended to its maximum length, which is known as bubble breakup length, the bubble breaks into two discrete daughter bubbles, as shown in Fig. 4.7 (i). After the breakup occurs, both the daughter bubble starts to move into both the branches of the T-junction opposite to each other, as shown in Fig. 4.7 (j-l). After some time, both the daughter bubbles obtained the shape similar to that of the parent bubble, as shown in Fig. 4.7 (m). In this way, the Taylor bubble breakup occurs for this case.

In this case, it is found that the length of the right side bubble is less than that of left side bubble, as shown in Fig. 4.7 (m). So it is an asymmetrical breakup process. It is also found that the bubble breakup length is more than that obtained in the previous cases. The breakup time for this case is maximum. Same process obtained for all the Taylor bubbles that are come from the upstream T-junction towards the downstream T-junction bifurcation.

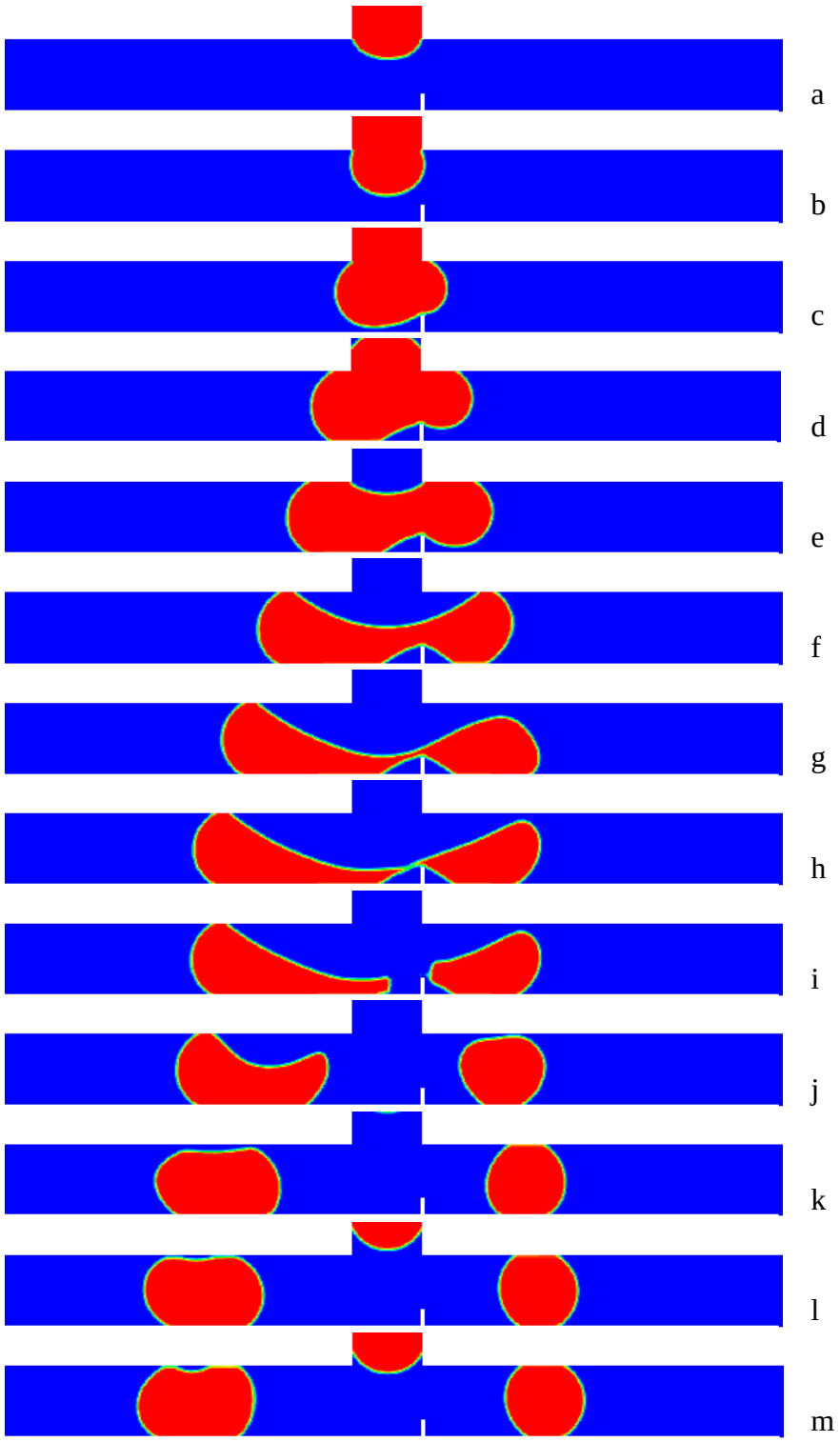

Fig. 4.7. Taylor bubble breakup process, when the obstacle positioned at X = 0.1 mm.

4.3.2. Varying obstacle height at constant position:

In this case, the position of the obstacle keeps constant, and the height is varied. For this the position of the obstacle taken as X = 0 mm (i.e. at the center of the T-junction bifurcation). Moreover, the height is varied towards the right side branch as Y= 0.05, 0.1, 0.15, and 0.2 mm.

4.3.2.1. Obstacle height Y = 0.05 mm:

In this case, the obstacle is positioned at the center of the T-junction bifurcation with a height of 0.05 mm. The image sequence of complete Taylor bubble breakup process is presented in Fig. 4.8. Before entering into the T-junction, the Taylor bubble is in symmetrical shape, as shown in Fig 4.8 (a). When the bubble enters into the T-junction, the shape of the bubble changes. As the obstacle positioned at the center of the T-junction, the tip of the front meniscus first touches the tip of the obstacle, as shown in Fig. 4.8 (b-c). After touching the obstacle the bubble started to move towards both the branches of the T-junction and developed two independent meniscus of the same size, as shown in Fig 4.8 (c). The flow rate of water in this case, is same in both the branches. Both the meniscus starts moving forward in opposite to each other, as shown in Fig 4.8 (d-e). Due to this the bubble length extended as time increases and the middle part of the bubble get thinner, as shown in Fig. 4.8 (f-h). After extended to its maximum length, which is known as bubble breakup length, the bubble breaks into two discrete daughter bubbles, as shown in Fig. 4.8 (i). After the breakup occurs, both the daughter bubble starts to move in both the branches of the T-junction opposite to each other, as shown in Fig. 4.8 (j-l). After some time, both the daughter bubbles obtained the shape similar to that of the parent bubble, as shown in Fig. 4.8 (m). From this case, it is found that both the daughter bubbles have the same length. So it is a symmetrical breakup process. The bubble breakup length in this case, is maximum, for this position of the obstacle.

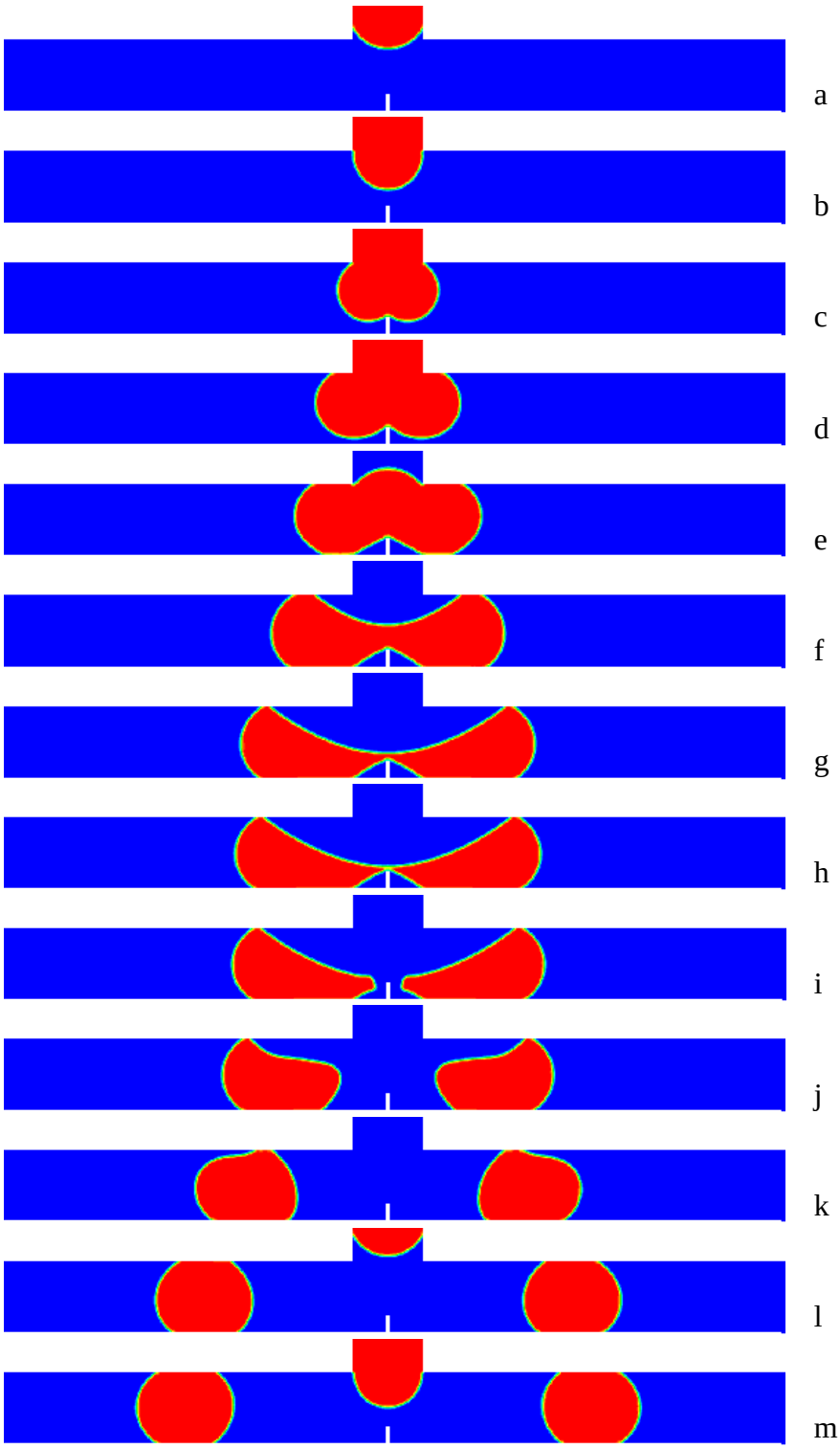

Fig. 4.8. Taylor bubble breakup process, when the obstacle height Y = 0.05 mm.

4.3.2.2. Obstacle height Y = 0.1 mm:

In this case, the obstacle is positioned at the center of the T-junction bifurcation with a height of 0.1 mm. The image sequence of complete Taylor bubble breakup process is presented in Fig. 4.9. Before entering into the T-junction, the Taylor bubble is in symmetrical shape, as shown in Fig 4.9 (a). As the obstacle positioned at the center of the T-junction, the tip of the front meniscus first touches the tip of the obstacle, as shown in Fig. 4.9 (b). After touching the obstacle, the bubble started to move towards both the branches of the T-junction and developed two independent meniscus of the same size, as shown in Fig 4.9 (c). The flow rate of water in this case, is same in both the branches. Both the meniscus starts moving forward in opposite to each other, as shown in Fig 4.9 (d-e). Due to this the bubble length extended as time increases and the middle part of the bubble get thinner, as shown in Fig. 4.9 (f-h). After extended to its maximum length, which is known as bubble breakup length, the bubble breaks into two discrete daughter bubbles, as shown in Fig. 4.9 (i). After the breakup occurs, both the daughter bubble starts to move in both the branches of the T-junction opposite to each other, as shown in Fig. 4.9 (j-l). After some time, both the daughter bubbles obtained the shape similar to that of the parent bubble, as shown in Fig. 4.9 (m). In this way, the Taylor bubble breakup occurs for this case.

From this case, it is found that both the daughter bubbles have the same length, as shown in Fig. 4.9 (m). So it is a symmetrical breakup process. The bubble breakup length in this case is less than that of in previous case, for this position of the obstacle. Also, the time taken for the breakup of the bubble is less than that of in the previous case. Same process obtained for all the Taylor bubbles that are come from the upstream T-junction towards the downstream T-junction bifurcation.

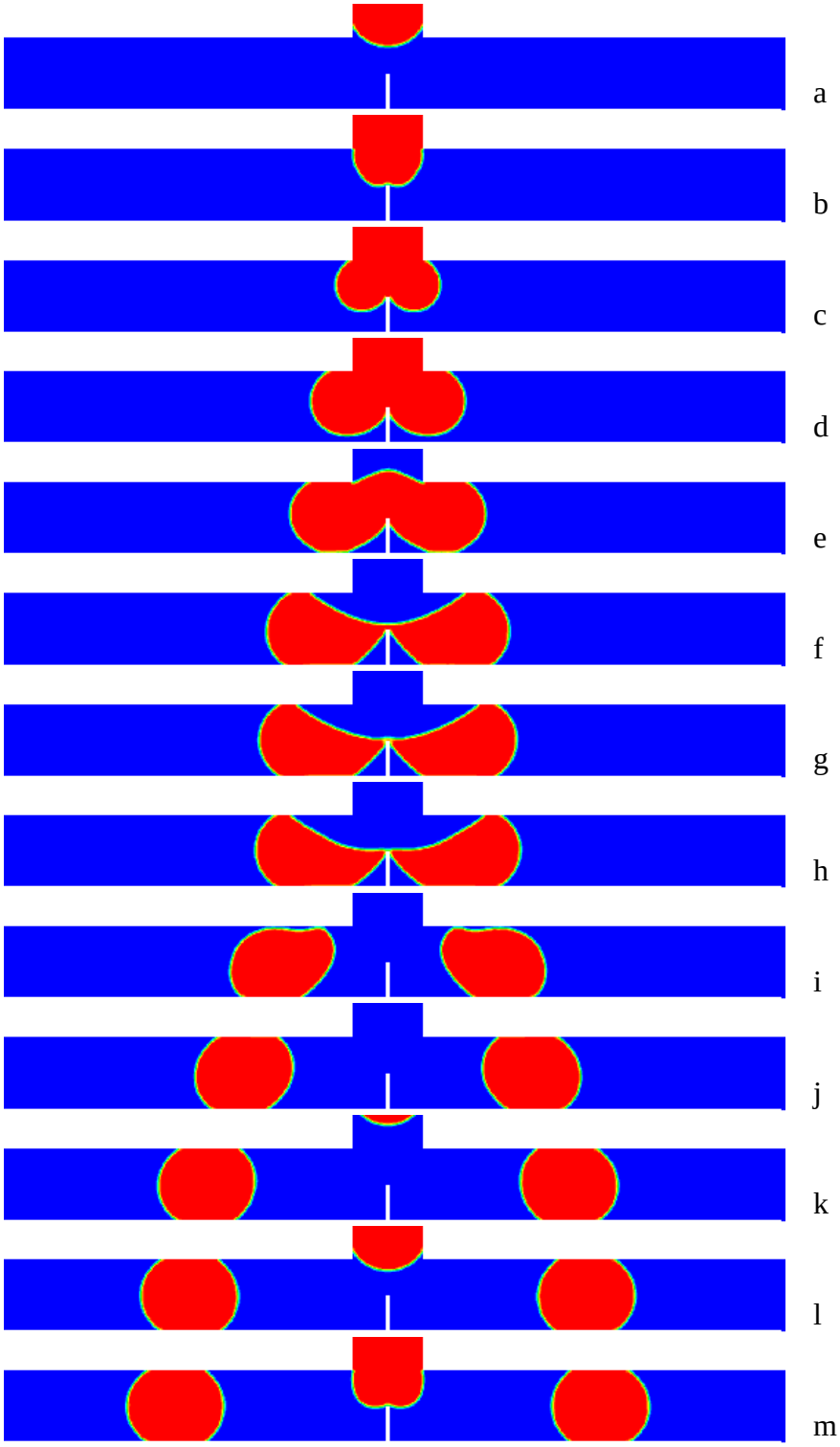

Fig. 4.9. Taylor bubble breakup process, when the obstacle height Y = 0.1 mm.

4.3.2.3. Obstacle height Y = 0.15 mm:

In this case, the obstacle is positioned at the center of the T-junction bifurcation with a height of 0.15 mm. The image sequence of complete Taylor bubble breakup process is presented in Fig. 4.10. Before entering into the T-junction, the Taylor bubble is in symmetrical shape, as shown in Fig 4.10 (a). As the obstacle positioned at the center of the T-junction, the tip of the front meniscus first touches the tip of the obstacle, as shown in Fig. 4.10 (b). After touching the obstacle, the bubble started to move towards both the branches of the T-junction and developed two independent meniscus of the same size, as shown in Fig 4.10 (c). The flow rate of water in this case is same in both the branches. Both the meniscus starts moving forward in opposite to each other, as shown in Fig 4.10 (d-f). Due to this, the bubble length extended as time increases and the middle part of the bubble get thinner, as shown in Fig. 4.10 (g-i). After extended to its maximum length, which is known as bubble breakup length, the bubble breaks into two discrete daughter bubbles, as shown in Fig. 4.10 (j). After the breakup occurs, both the daughter bubble starts to move in both the branches of the T-junction opposite to each other, as shown in Fig. 4.10 (k-l). After some time, both the daughter bubbles obtained the shape similar to that of the parent bubble, as shown in Fig. 4.10 (m). In this way, the Taylor bubble breakup occurs for this case.

From this case, it is found that both the daughter bubbles have the same length, as shown in Fig. 4.10 (m). So it is a symmetrical breakup process. The bubble breakup length in this case is less than that of in previous cases, for this position of the obstacle. Also, the time taken for the breakup of the bubble is less than that of in the previous cases. Same process obtained for all the Taylor bubbles that are come from the upstream T-junction towards the downstream T-junction bifurcation.

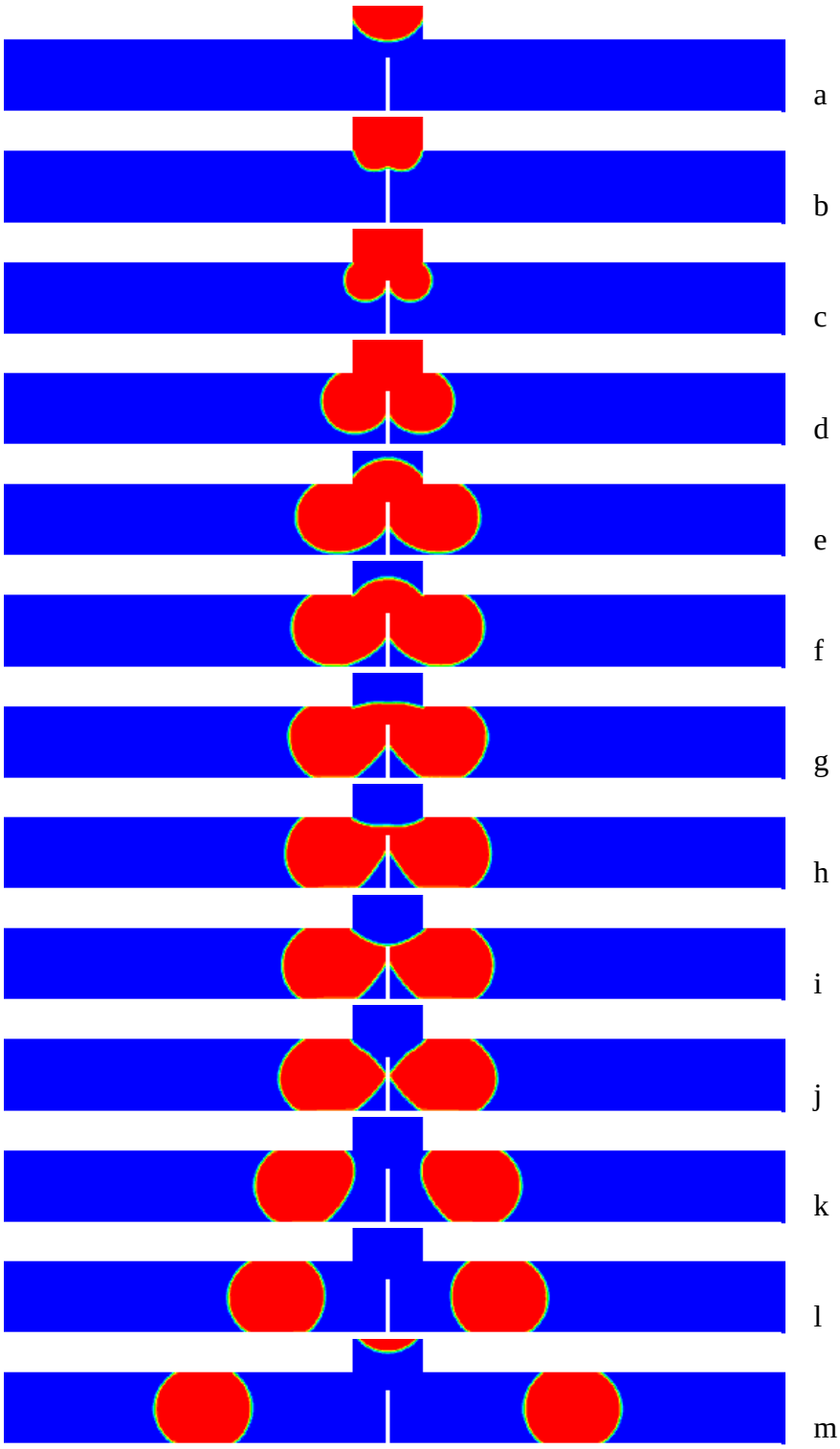

Fig. 4.10. Taylor bubble breakup process, when the obstacle height Y = 0.15 mm.

4.3.2.3. Obstacle height Y = 0.2 mm:

In this case, the obstacle is positioned at the center of the T-junction bifurcation with a height of 0.2 mm. The image sequence of complete Taylor bubble breakup process is presented in Fig. 4.11. Before entering into the T-junction, the Taylor bubble is in symmetrical shape, as shown in Fig. 4.11 (a). As the obstacle positioned at the center of the T-junction, the tip of the front meniscus first touches the tip of the obstacle, as shown in Fig. 4.11 (b). After touching the obstacle, the bubble started to move towards both the branches of the T-junction and developed two independent meniscus of the same size, as shown in Fig. 4.11 (c). The flow rate of water in this case is same in both the branches. Both the meniscus starts moving forward in opposite to each other, as shown in Fig. 4.11 (d-f). Due to this, the bubble length extended as time increases and the middle part of the bubble get thinner, as shown in Fig. 4.11 (g-i). After extended to its maximum length, which is known as bubble breakup length, the bubble breaks into two discrete daughter bubbles, as shown in Fig. 4.11 (j). After the breakup occurs, both the daughter bubble starts to move in both the branches of the T-junction opposite to each other, as shown in Fig. 4.11 (k-l). After some time, both the daughter bubbles obtained the shape similar to that of the parent bubble, as shown in Fig. 4.11 (m). In this way, the Taylor bubble breakup occurs for this case.

From this case, it is found that both the daughter bubbles have the same length, as shown in Fig. 4.11 (m). So it is a symmetrical breakup process. The bubble breakup length in this case is less than that of in previous cases, for this position of the obstacle. Also, the time taken for the breakup of the bubble is less than that of in the previous cases. Same process obtained for all the Taylor bubbles that are come from the upstream T-junction towards the downstream T-junction bifurcation.

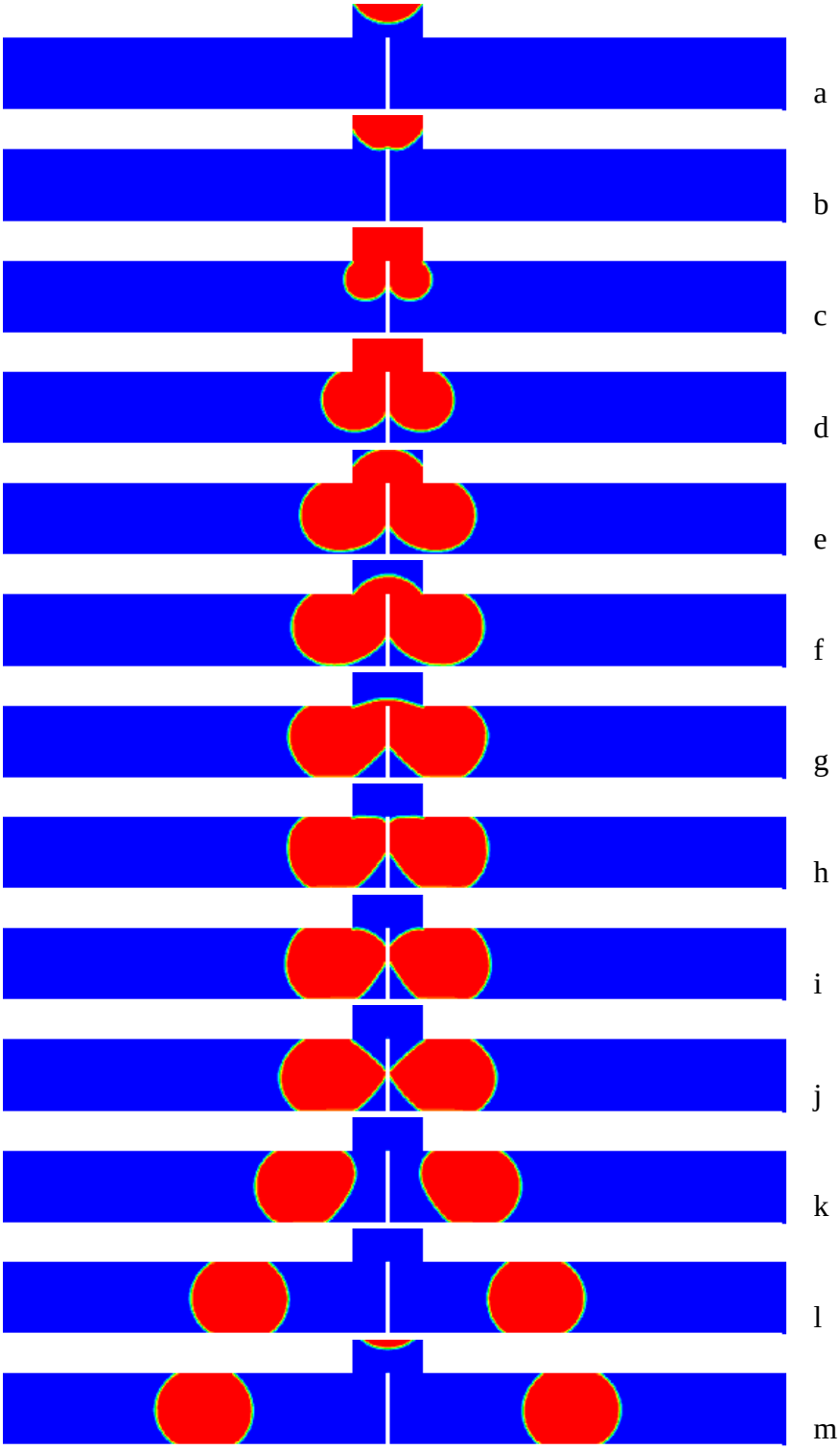

Fig. 4.11. Taylor bubble breakup process, when the obstacle height Y = 0.2 mm.

4.4. Different parameter calculation:

In this section, different parameters such as bubble length ratio, bubble breakup length, bubble breakup time and pressure drop are discussed. Some graphs are plotted between these parameters and the height of the obstacle at different obstacle position. For calculation of these parameters different cases are simulated by varying obstacle height as (Y = 0.05, 0.1, 0.15 and 0.2 mm) and by varying obstacle position as (X = 0, 0.025, 0.05, 0.075 and 0.1 mm).

4.4.1. Bubble length ratio:

After the breakup of the parent Taylor bubble, two new daughter bubbles are formed and move into both the branches of the T-junction bifurcation. These daughter bubbles having length less than that of the parent bubble. The bubble length ratio is defined as the ratio between the lengths of the bubble in right side branch to that of in left side branch, as shown in Fig. 4.12.

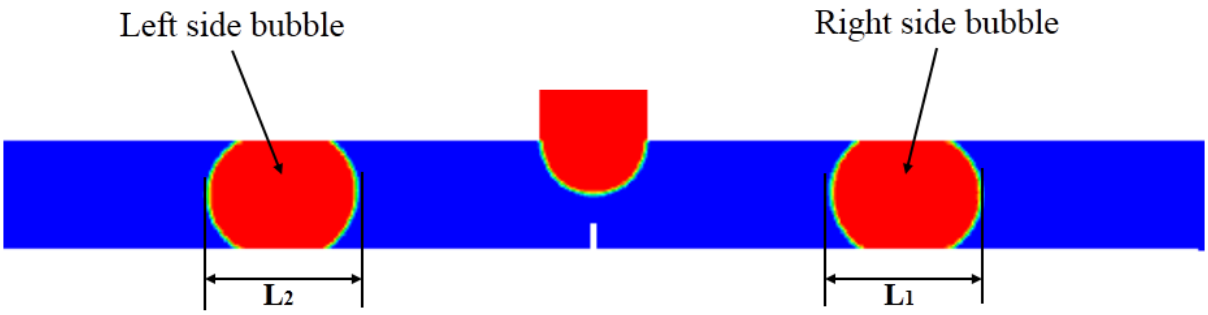

Fig. 4.12. Daughter bubbles in right and left branches.

From this figure, the bubble length ratio can be calculated by calculating individual bubble length. This bubble length ratio is calculated for all the cases and finding out the variations for different case by plotting a graph, as shown in Fig. 4.13. This figure illustrates the bubble length ratio as a function of obstacle height at different obstacle position. From this plot, it is found that, when the obstacle is positioned at the center (X = 0 mm), the bubble length ratio is independent of the obstacle height. This because, in this the bubble breaks into two equal daughter bubbles. For other position of the obstacle, the bubble length ratio decreases as the obstacle height increases.

This because, in these cases asymmetrical breakup occurs. From this plot, it is also found that for the position of X = 0.075 and 0.1 mm there are no value for bubble length ratio at the height of Y = 0.2 mm. In these two cases, the single bubble move into the left branch instead of breaking, because the obstacle block the flow to the right channel, as shown in Fig. 4.14. It can also discuss in a reverse way that, for a particular obstacle height the bubble length ratio decreases as the obstacle position increases (except X = 0 mm).

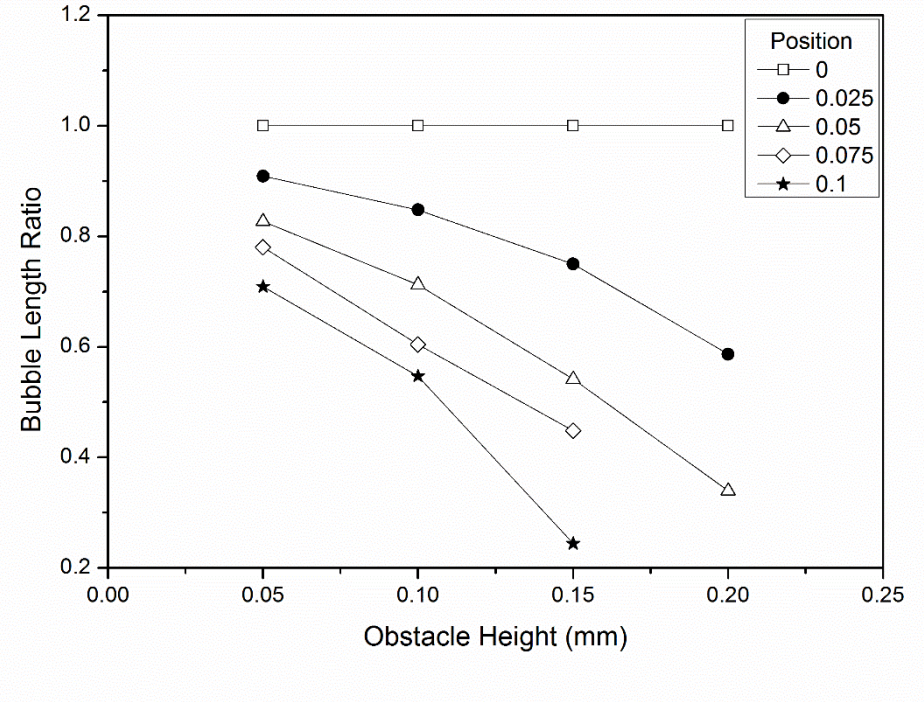

Fig. 4.13. Bubble length ratio as a function of obstacle height at different obstacle position.

Fig. 4.14. Single bubble flow, at X = 0.075 mm and Y = 0.2 mm.

4.4.2. Bubble breakup length:

The bubble breakup length is defined as the distance between the ends of the bubble at the breakup moment, or we can say just before the breakup, as shown in Fig. 4.15. It is also known as the maximum length that a bubble can extend just before the breakup. This bubble breakup length is calculated for all the cases and plotted a graph with respect to the obstacle height for different position of the obstacle, as shown in Fig. 4.16.

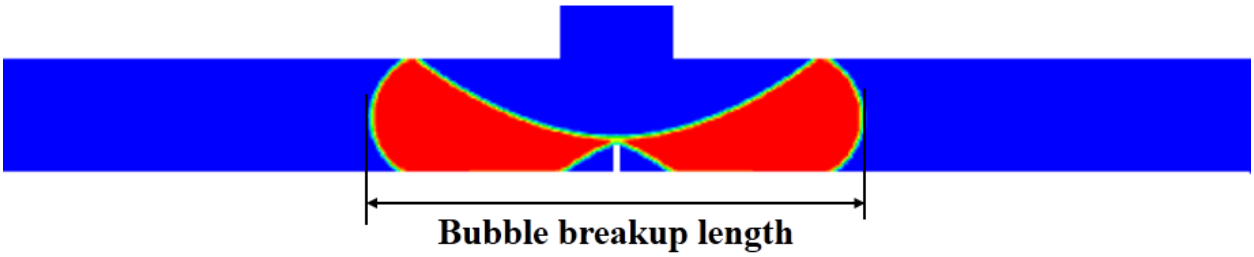

Fig. 4.15. Bubble breakup length just before the breakup.

The Fig. 4.16 describes the bubble breakup length as a function of obstacle height at different obstacle position. From this graph, it is observed that, for a particular position of the obstacle the bubble breakup length decreases as the obstacle height increases. The initial bubble breaks into unequal parts (except X = 0 mm), so there exists two breakup length one is smaller part breakup length in the right branch and other is larger part breakup length in the left branch. From this, it is also observed that for a particular obstacle height, the bubble breakup length increases as the position of the obstacle increases. The maximum bubble breakup length obtained for the case in which the obstacle height is Y = 0.05 mm and obstacle position at X = 0.1 mm. When the obstacle positioned at (X = 0.075 and 0.1 mm) and the obstacle height is Y = 0.2 mm, the bubble does not break. So for these two cases no bubble breakup length calculated.

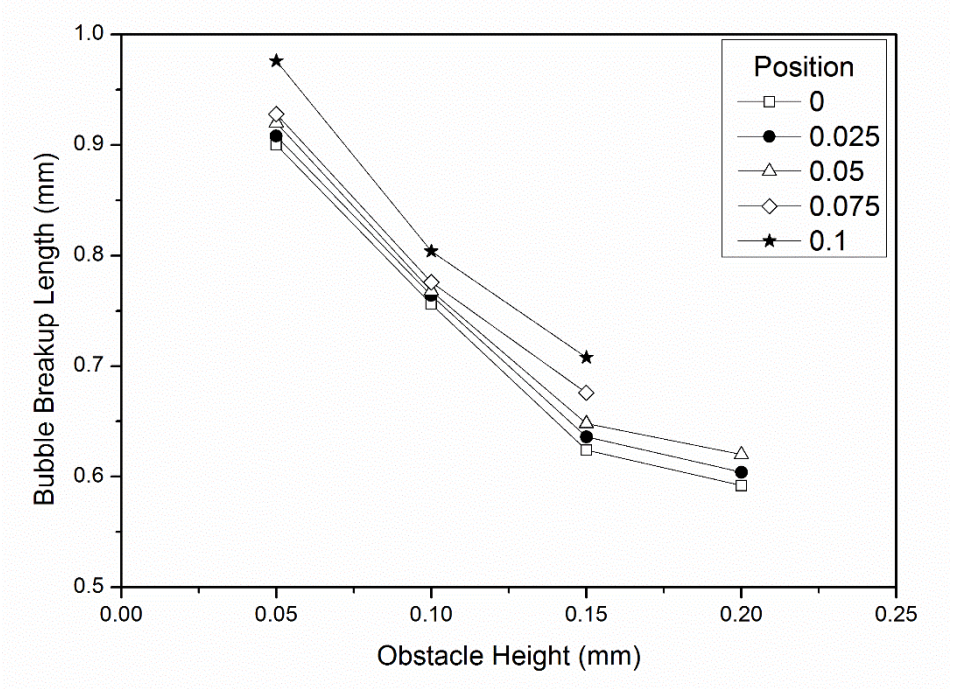

Fig. 4.16. Bubble breakup length as a function of obstacle height at different obstacle position.

4.4.3. Bubble breakup time:

The bubble breakup time is defined as the time between the moment that the bubble touches the tip of the obstacle (Fig. 4.17 (a)) and the moment that the bubble breaks up (Fig. 4.17 (b)).

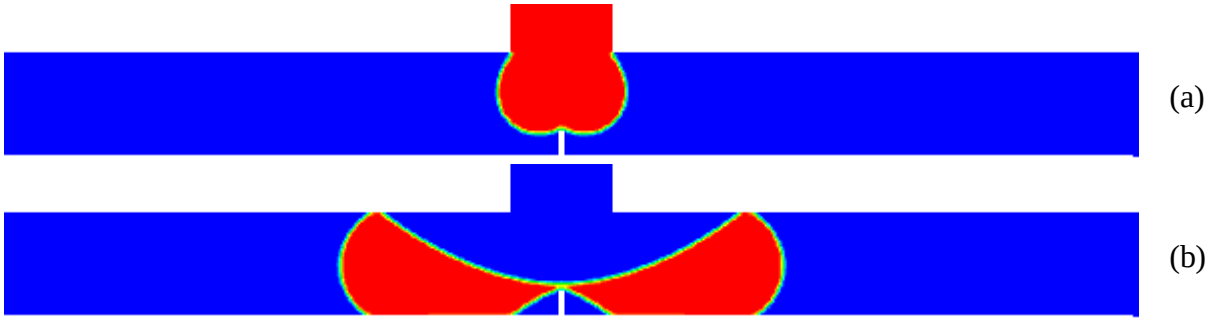

Fig. 4.17. (a) Shows the moment that the bubble just touch the obstacle, (b) Shows the moment that the bubble just breaks up.

Fig. 4.18 displays the bubble breakup time as a function of the obstacle height for different position of the obstacle. From this graph, it is seen that the bubble breakup time decreases as the obstacle height increases for a particular obstacle position. It is because when the height of the obstacle increases the time at which the bubble touches the obstacle decreases. It can also explain from this graph that for a particular obstacle height, the bubble breakup time increases as the position of the obstacle shifted to the right side (i.e. X increases). The maximum bubble breakup time obtained for the case in which the obstacle height (Y = 0.05 mm) and the obstacle positioned at (X = 0.1 mm). It is also found that for the obstacle height of 0.2 mm the bubble takes very less time for the breakup. When the obstacle positioned at (X = 0.075 and 0.1 mm) and the obstacle height is Y = 0.2 mm, the bubble does not break. So for these two cases bubble breakup time is not calculated.

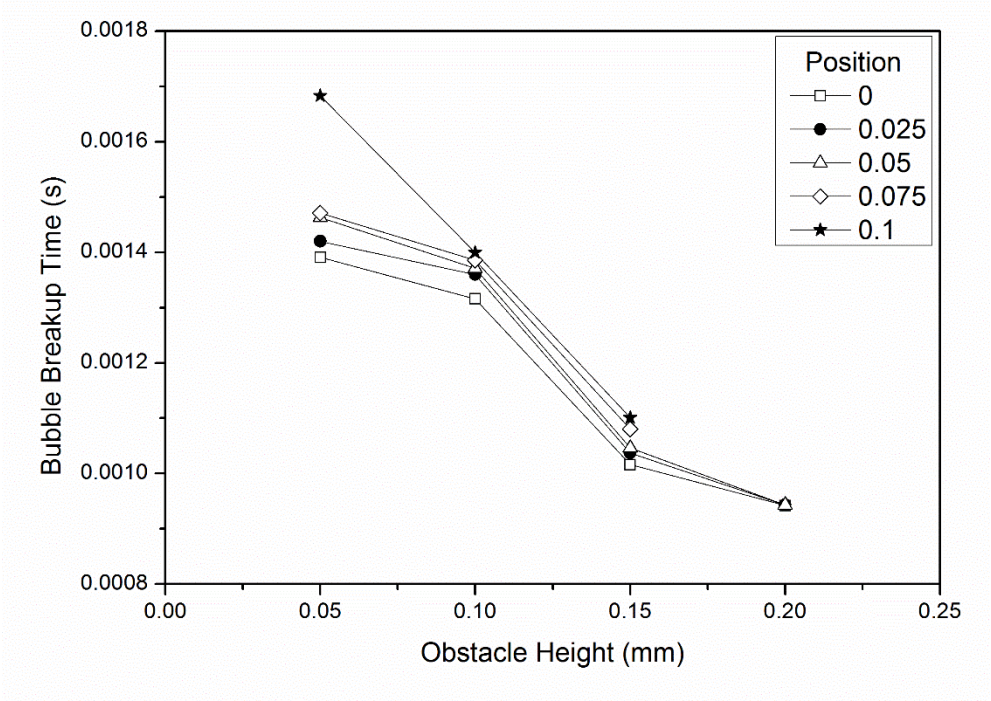

Fig. 4.18. Bubble breakup time as a function of obstacle height at different obstacle position.

4.4.4. Pressure drop:

The pressure drop plays a crucial role in the microfluidic systems. In this work, the pressure drop was calculated at the moment of bubble breakup, as shown in Fig. 4.19. For calculating pressure drop, first the individual pressures are calculated at three sections, as shown in Fig. 4.19. Moreover, then the pressure drop calculated in a dimensionless form that is given below.

$$p^* = \frac{p_i - p_r}{p_i - p_l}$$

where p* is the dimensionless pressure drop, p_i is the pressure at a section before T-junction, p_r is pressure at a section in the right branch, and p_l is the pressure at a section in the left branch.

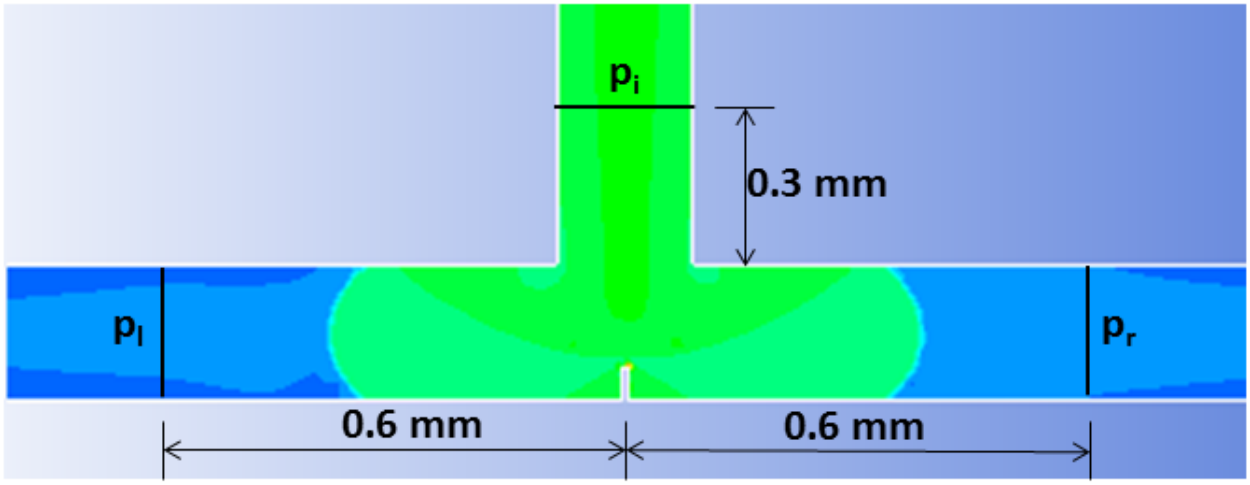

Fig. 4.19. Pressure contour at the moment of bubble breakup.

Fig. 4.20 displays the pressure drop as a function of the obstacle height at different position of the obstacle. From this graph, it is found that the pressure drop increases as the obstacle height increases. However, when the obstacle is positioned at the center of the T-junction the pressure drop does not change significantly with respect to the obstacle height. In case of other obstacle positioning the pressure drop is increased because, at the time of bubble breakup there is smaller part of the bubble present on the right side branch and larger part of the bubble present on the left

side branch. Due to this there is more amount of water present inside right side branch than that of in the left side branch. We know that water is more viscous than air, so in which side amount of water is more on that side the pressure drop is more. From this, it is understood that the pressure drop in right side branch is more than that of in left side branch. As obstacle height increases the pressure drop in right side branch also increases, due to which the overall pressure drop is increased.

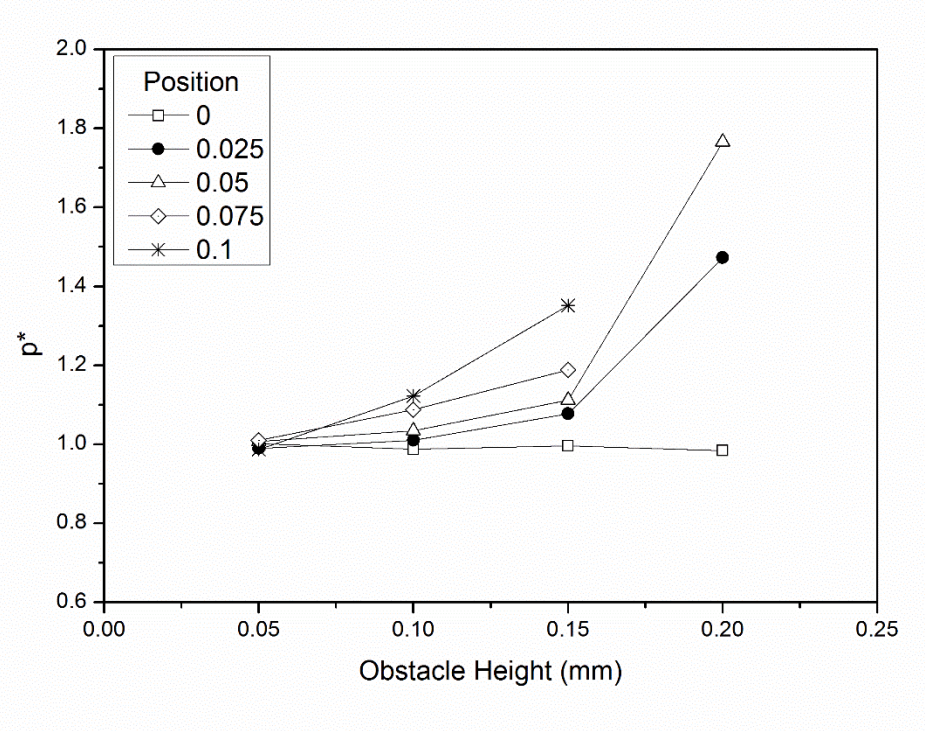

Fig. 4.20. Pressure drop as a function of the obstacle height at different position of the obstacle.

When the obstacle is positioned at (X = 0.075 mm and 0.1 mm), and the obstacle height is 0.2 mm, there is no pressure drop calculation occurs. This because, in these situations there is no bubble breakup takes place. From this graph, it is also observed that the pressure drop increases as the position of the obstacle increases for a particular obstacle height.

Chapter-5

Conclusion

A two-dimensional numerical study of Taylor bubble breakup is carried out, where the Taylor bubble flows in a horizontal T- section microchannel with T-junction bifurcation. An obstacle is positioned at the T-junction bifurcation for the breakup of the Taylor bubble. By varying the position and height of the obstacle, the bubble size can controlled according to the requirement.

The numerical simulation is carried out using the Volume-of-Fluid (VOF) multiphase model in ANSYS Fluent®. The results of the Taylor bubble breakup by using obstacle at T-junction bifurcation were presented. By varying obstacle position and height different parameters, were obtained, such as bubble length ratio, bubble breakup length, bubble breakup time and pressure drop. The results revealed that as the obstacle height increased for a particular obstacle position, the bubble length ratio is decreased. However, when the obstacle is at the center of the T-junction bifurcation, the bubble length ratio is constant. Because, in this case, the bubble breaks into two equal sized daughter bubble. The unequal length in bubble arises due to the difference in resistance to flow along the bifurcated channels. The resistance to flow will be more along the bifurcated channel along which the obstacle is positioned. So the bubble length is smaller along this outlet. Also, it was found that the bubble breakup length decreases as the obstacle height increases for a particular obstacle position. It also found that as the obstacle height increases the bubble breakup time decreases for a particular position of the obstacle. The influence of the obstacle position and

height on the pressure drop of the system was also studied, and it was found that by increasing the height of the obstacle the pressure drop increases for a particular obstacle position. From these different cases, it was also found that when the obstacle positioned at X = 0.075 and 0.1 mm and the height Y = 0.2 mm there is no breakup occurs. It is because in these two cases, the Taylor bubble does not find a way to flow into the right side branch, only a single bubble flow into the left side branch of the T-junction bifurcation. From this work, it was concluded that by varying obstacle position and height the size of the bubble can be controlled accordingly.

References:

[1] Gibson, A. H., (1913). On the motion of long air-bubbles in a vertical tube. Philosophical Magazine Series 6, 26(156), pp. 952-965.

[2] Fair brother, F., and Stubbs, A. E., (1935). Studies in electro-endosmosis. Part VI. The bubble-tube method of measurement. Journal of the Chemical Society, 1, pp. 527–529.

[3] Triplett, K.A., Ghiaasiaan, S.M., Abdel- Khalik, S.I., and Sadowski, D.L., (1999). Gas–liquid two-phase flow in micro channels. International Journal of Multiphase Flow, vol. 25, no. 3, pp. 377–394.

[4] Zhao, T.S. and Bi, Q.C., (2001). Co-current air–water two phase flow patterns in vertical triangular micro channels. International Journal of Multiphase Flow, vol. 27, no. 5, pp.765–782.

[5] Liu H., Vandu C.O., Krishna R., (2005). Hydrodynamics of Taylor flow in vertical capillaries: Flow regimes, bubble rise velocity, liquid slug length, and pressure drop. Industrial & Engineering Chemistry Research 44, 4884–4897.

[6] Qian, D., and Lawal, A., (2006). Numerical study on gas and liquid slugs for Taylor flow in a T-junction micro channel. Chemical Engineering Science 61, pp. 7609-7625.

[7] Santos, R. M., and Kawaji, M., (2010). Numerical modeling and experimental investigation of gas-liquid slug formation in a microchannel T-junction. International Journal of Multiphase Flow, 36(4), pp. 314-323.

[8] Zhang T, Cao B., Fan Y., Gonthier Y., Luo L., Wang S., (2011). Gas liquid flow in circular micro channel. Part.1- Influence of liquid physical properties and channel diameter on flow patterns. Chemical Engineering Science 66, 5791-5803.

[9] Pham, H., Wen, L., and Zhang, H., (2012). Numerical simulation and analysis of gas liquid flow in a T-junction microchannel. Advanced Mechanical Engineering, pp. 1-8.

[10] Bretherton, F. P., (1961). The motion of long bubbles in tubes. Journal of Fluid Mechanics, 10(2), pp 166-188.

[11] Gupta, R., Fletcher, D. F., and Haynes, B. S., (2009). On the CFD modelling of Taylor flow in microchannels. Chemical Engineering. Science, 64(12), pp. 2941-2950.

[12] Kang, S., & Zhou, B. (2014). Numerical study of bubble generation and transport in a serpentine channel with a T-junction. International Journal of Hydrogen Energy, 39(5), 2325-2333.

[13] Thippavathini, S., & Moharana, M. K. (2014, August). Flow of Taylor bubble in microchannel having an obstacle. In ASME 2014 12th International Conference on Nanochannels, Microchannels, and Minichannels collocated with the ASME 2014 4th Joint US-European Fluids Engineering Division Summer Meeting (pp. V001T03A012-V001T03A012). American Society of Mechanical Engineers.

[14] Dang, M., Yue, J., & Chen, G. (2015). Numerical simulation of Taylor bubble formation in a microchannel with a converging shape mixing junction. Chemical Engineering Journal, 262, 616-627.

[15] Thorsen, T., Roberts, R. W., Arnold, F. H., & Quake, S. R. (2001). Dynamic pattern formation in a vesicle-generating microfluidic device. Physical Review Letters, 86(18), 4163.

[16] Stone, H. A., Stroock, A. D., & Ajdari, A. (2004). Engineering flows in small devices: microfluidics toward a lab-on-a-chip. Annual Review of Fluid Mechanics, 36, 381-411.

[17] Tice, J. D., Song, H., Lyon, A. D., & Ismagilov, R. F. (2003). Formation of droplets and mixing in multiphase microfluidics at low values of the Reynolds and the capillary numbers. Langmuir, 19(22), 9127-9133.

[18] Link, D. R., Anna, S. L., Weitz, D. A., & Stone, H. A. (2004). Geometrically mediated breakup of drops in microfluidic devices. Physical Review Letters, 92(5), 054503.

[19] Garstecki, P., Fuerstman, M. J., Stone, H. A., & Whitesides, G. M. (2006). Formation of droplets and bubbles in a microfluidic T-junction-scaling and mechanism of break-up. Lab on a Chip, 6(3), 437-446.

[20] Jousse, F., Farr, R., Link, D. R., Fuerstman, M. J., & Garstecki, P. (2006). Bifurcation of droplet flows within capillaries. Physical Review E, 74(3), 036311.

[21] Ting, T. H., Yap, Y. F., Nguyen, N. T., Wong, T. N., Chai, J. C. K., & Yobas, L. (2006). Thermally mediated breakup of drops in microchannels. Applied Physics Letters, 89(23), 234101.

[22] Ménétrier-Deremble, L., & Tabeling, P. (2006). Droplet breakup in microfluidic junctions of arbitrary angles. Physical Review E, 74(3), 035303.

[23] Choi, J. H., Lee, S. K., Lim, J. M., Yang, S. M., & Yi, G. R. (2010). Designed pneumatic valve actuators for controlled droplet breakup and generation. Lab Chip, 10(4), 456-461.

[24] Zhu, H. W., Zhang, N. G., He, R. X., Li, S. Z., Guo, S. S., Liu, W., & Zhao, X. Z. (2011). Controllable fission of droplets and bubbles by pneumatic valve. Microfluidics and Nanofluidics, 10(6), 1343-1349.

[25] Bedram, A., & Moosavi, A. (2011). Droplet breakup in an asymmetric microfluidic T junction. The European Physical Journal E: Soft Matter and Biological Physics, 34(8), 1-8.

[26] Wu, Y., Fu, T., Zhu, C., Lu, Y., Ma, Y., & Li, H. Z. (2012). Asymmetrical breakup of bubbles at a microfluidic T-junction divergence: feedback effect of bubble collision. Microfluidics and Nanofluidics, 13(5), 723-733.

[27] Bedram, A., & Moosavi, A. (2012). Breakup of Droplets in Micro and Nanofluidic T-Junctions. Applied Mechanics and Materials, 110, 3673-3678.

[28] Hoang, D. A., Portela, L. M., Kleijn, C. R., Kreutzer, M. T., & Van Steijn, V. (2013). Dynamics of droplet breakup in a T-junction. Journal of Fluid Mechanics, 717, R4.

[29] Bedram, A., Darabi, A. E., Moosavi, A., & Hannani, S. K. (2015). Numerical Investigation of an Efficient Method (T-Junction with Valve) for Producing Unequal-Sized Droplets in Micro-and Nano-Fluidic Systems. Journal of Fluids Engineering, 137(3), 031202.